Mnk1/2 kinases regulate memory and autism-related behaviours via Syngap1

Kleanthi Chalkiadaki,[1,2,†] Mehdi Hooshmandi,[3,†] Gilliard Lach[2,4,†] Elpida Statoulla,[1] Konstanze Simbriger,[2,‡] Ines S. Amorim,[2] Stella Kouloulia,[2,§] Maria Zafeiri,[1] Panagiotis Pothos,[1] Éric Bonneil,[5] Ilse Gantois,[6] Jelena Popic,[6] Sung-Hoon Kim,[6] Calvin Wong,[3] Ruifeng Cao,[7,8] Noboru H. Komiyama,[4,9] Yaser Atlasi,[10] Seyed Mehdi Jafarnejad,[10,#] Arkady Khoutorsky[4,#] and Christos G. Gkogkas[1,#]

[†,#]**These authors contributed equally to this work.**

Abstract

MAPK (mitogen-activated protein kinase) interacting protein kinases 1 and 2 (Mnk1/2) regulate a plethora of functions, presumably via phosphorylation of their best characterised substrate, eukaryotic translation initiation factor 4E (eIF4E) on Ser209. Here, we show that whereas deletion of *Mnk1/2* (Mnk DKO) impairs synaptic plasticity and memory in mice, ablation of phosho-eIF4E (Ser209) does not affect these processes, suggesting that Mnk1/2 possess additional downstream effectors in the brain. Translational profiling revealed only a small overlap between Mnk1/2- and phospho-eIF4E(Ser209)-regulated translatome. We identified the synaptic Ras GTPase activating protein 1 (Syngap1), encoded by a syndromic autism gene, as a downstream target of Mnk1 since Syngap1 immunoprecipitated with Mnk1 and showed reduced phosphorylation (S788) in Mnk DKO mice. Knock-down of Syngap1 reversed memory deficits in Mnk DKO mice, and pharmacological inhibition of Mnks rescued autism-related phenotypes in *Syngap1*$^{+/-}$ mice. Thus, Syngap1 is a downstream effector of Mnk1, and the Mnks-Syngap1 axis regulates memory formation and autism-related behaviours.

Author affiliations:

1 Biomedical Research Institute, Foundation for Research and Technology-Hellas, University Campus, 45110 Ioannina, Greece

2 Centre for Discovery Brain Sciences and The Patrick Wild Centre, University of Edinburgh, EH8 9XD, Edinburgh, Scotland, UK

3 Department of Anesthesia and Alan Edwards Centre for Research on Pain, McGill University, H3A 0G1, Montréal, QC, Canada

4 Simons Initiative for the Developing Brain, University of Edinburgh, EH8 9XD, Edinburgh, Scotland, UK

5 Institute for Research in Immunology and Cancer, Université de Montréal, P.O. Box 6128, Station Centreville, Montréal, Québec H3C 3J7, Canada

6 Goodman Cancer Institute and Biochemistry Department, McGill University, H3A 1A3, Montréal, QC, Canada

7 Department of Biomedical Sciences, University of Minnesota Medical School, Duluth, MN 55812, USA.

8 Department of Neuroscience, University of Minnesota Medical School, Minneapolis, MN 55455, USA

9 Genes to Cognition Program, Centre for Clinical Brain Sciences, University of Edinburgh, Edinburgh EH16 4SB, UK

10 Pathrick G. Johnston Centre for Cancer Research, The Queen's University of Belfast, BT9 7AE, Belfast, Northern Ireland, UK

[‡]Present address: Department of Pharmacology, Medical University Innsbruck, 6020, Innsbruck, Austria

[§]Present address: MRC Laboratory for Molecular Cell Biology, University College London, Gower Street, London WC1E 6BT, UK

Correspondence to: Christos G. Gkogkas

Biomedical Research Institute, Foundation for Research and Technology-Hellas, University Campus, 45110 Ioannina, Greece

E-mail: cgkogkas@bri.forth.gr

Running title: The Mnk-Syngap1 axis in memory and autism

Keywords: translational control; learning; memory; autism; synaptic translation; phosphorylation

Introduction

Downstream of Ras/ERK (extracellular regulated kinase) and p38 (mitogen-activated protein kinase) MAPK pathways, MAPK interacting protein kinase1 (Mnk1) and Mnk2 exert a plethora of biological functions in response to external stimuli (*e.g.*, mitogens) and internal cues[1,2]. Only a few substrates are known for Mnk1/2 kinase activity, of which the best described is the Ser209 residue on the eukaryotic translation initiation factor 4E (eIF4E), which is involved in the regulation of cap-dependent translation[1]. Indeed, in most tissues and cell types examined, phospho-eIF4E (Ser209) is considered the key downstream effector of Mnks. Activation of Mnk1 enhances its binding to the eukaryotic initiation factor 4G (eIF4G) and promotes phosphorylation of eIF4E. In addition, eIF4E forms a complex with eIF4A and eIF4G (called eIF4F) to facilitate ribosome recruitment and promote translation initiation[2].

mRNA translation downstream of Mnks was shown to be important for tumorigenesis, inflammation, immunity, Internal Ribosome Entry Site (IRES)-mediated translation initiation and resistance to anti-cancer drugs (*e.g.*, inhibitors of mechanistic Target of Rapamycin (mTOR))[3].

In the brain, downstream of MAPKs, Mnks were hypothesised to regulate synaptic plasticity, learning, memory, and other behaviours via eIF4E[4,5]. Accumulating evidence highlights a role for Mnks in fragile X syndrome (FXS) and autism spectrum disorder (ASD). Mnk1 was shown to regulate translation of mRNAs involved in neurotransmission and synaptic plasticity, a significant subset of which overlaps with proteins regulated by fragile X messenger ribonucleoprotein (Fmrp)[6]. In addition, genetic deletion or pharmacological inhibition of Mnks in a mouse model of FXS rescues core FXS-related behaviours as well as numerous cellular and molecular phenotypes[7]. A link between Mnks and ASD was recently strengthened by demonstrating that pharmacological inhibition of Mnk restores mRNA translation, oxytocin signalling and social novelty responses in a mouse model of the syndromic ASD gene Neuroligin 3 (*Ngln3*)[8]. Strikingly, we previously demonstrated that mice harbouring an unphosphorylatable

Ser209Ala transgene (*Eif4e*^{Ser209Ala}) exhibit intact hippocampal long-term potentiation (LTP) and long-term memory[9], suggesting a role for additional Mnk downstream effectors, other than eIF4E, in these processes. Thus, despite the diverse roles and functions of Mnks, Mnks-mediated eIF4E phosphorylation cannot fully explain all processes under the control of Mnks in the brain, including learning and memory.

Here, we demonstrate that Mnks in the brain regulate learning, memory, and ASD-like behaviours via regulation of the syndromic ASD gene, synaptic Ras GTPase activating protein 1 (Syngap1), which controls mTOR Complex 1 (mTORC1) activity. First, we show that *Mnk1/2* deletion in mice (Mnk DKO)[10] impairs synaptic plasticity, learning, and memory, in contrast to phenotypes previously shown in *Eif4e*^{Ser209Ala} mice[9]. We reveal a small overlap between the differentially translated mRNAs in *Eif4e*^{Ser209Ala} and Mnk DKO mice brains, suggesting that substrates other than eIF4E dictate the effects of Mnks on brain functions. Second, we provide evidence that Mnks promote mTORC1 signalling and protein synthesis through interaction with and phosphorylation-dependent inhibition of Syngap1 by regulating its GAP (GTPase-accelerating protein) activity for Rheb (Ras homolog enriched in brain), a small GTPase upstream activator of mTORC1. Syngap1 acts as a repressor of protein synthesis and its deletion is known to lead to elevated mTORC1 signalling, increased global protein synthesis and autism-like behaviours[11-13]. Moreover, we show that manipulation of the Mnk-Syngap1 axis, using genetic or pharmacological approaches, normalizes altered mTORC1 signalling and corrects behavioural deficits in both Mnk DKO and *Syngap1*$^{+/-}$ mice. Thus, these data establish a previously unknown link between Mnks and Syngap1 upstream of translational control and demonstrate the important role of Mnks-Syngap1 axis in memory and autism-related behaviours, which is amenable to pharmacological manipulation.

Materials and methods

Animals

All procedures were in accordance with UK Home Office and Canadian Council on Animal Care regulations and were approved by the University of Edinburgh and McGill University. *Mnk1*$^{-/-}$ *Mnk2*$^{-/-}$, *Mnk1*$^{+/+}$*Mnk2*$^{+/+}$, *Syngap1*$^{+/+}$ *and Syngap1*$^{+/-}$ animals were backcrossed for more than

10 generations to C57Bl/6J background. Food and water were provided *ad libitum*. Pups were kept with their dams until weaning at postnatal day 21. After weaning, mice were group housed (maximum of 5 per cage) by sex. Cages were maintained in ventilated racks in temperature (20-21 ^{o}C) and humidity (~55%) controlled rooms, on a 12-hour circadian cycle (7am-7pm light period). Male and female mice were used (for Figures 1-5 only male mice were used, for Figure 6, 50% male and 50% female mice were used for all groups).

Four days before behavioural experiments, mice were handled for 30 min each day. On the day of the experiment, animals were transported from the housing room to the procedure room and habituated for 1 h before starting the test.

Morris Water Maze Test

Training in the pool (100 cm pool diameter and 10 cm diameter platform; water temperature was 24^{o}C, room at 20 lux) consisted of three trials per day (20 min inter-trial interval); each mouse was allowed to swim until it reached the hidden platform. Animals that did not find the platform after 60 s were gently guided to it and allowed to stay on the platform for 10 s prior to returning them to the cage. For the probe test on day 6, the platform was removed, and animals were allowed to swim for 60 s. The swimming trajectory and velocity were monitored with a video tracking system (HVS Image or ANY-maze, Stoelting, USA).

Contextual Fear Conditioning Test

Mice were, as described previously[9,14], conditioned in the chamber: 2 min acclimatization to the context, followed by the unconditioned stimulus (US); one foot shock (0.5 mA, 2 s) followed by a 30 s interval, terminating with another identical foot shock. The mice remained in the chamber for an additional 1 min after the end of the last US, after which they were returned to their home cages. Contextual fear memory was assayed 24 h after training by re-exposing the animals to the conditioning context for a 5-min period. During this period, the incidence of freezing response (absence of movement except for respiration) was recorded (FreezeFrame, Coulbourn Instruments). Freezing behaviour was analysed by assigning animals at 5 s intervals as either

freezing or not freezing. Data are expressed as the percentage of 5 s intervals scored as "freezing" (freezing behaviour during the session).

Extracellular Field Electrophysiology

Transverse hippocampal slices (400 μm) were prepared from WT (wild-type) or Mnk DKO male mice (6–8 weeks old). Slices were allowed to recover submerged for at least 2 h at 32°C in oxygenated artificial cerebrospinal fluid (ACSF) containing 124 mM NaCl, 2.5 mM KCl, 1.25 mM NaH_2PO_4, 26 mM $NaHCO_3$, 10 mM glucose, 1.3 mM $MgCl_2$, and 2.5 mM $CaCl_2$ before transferring to a recording chamber at 28°C–29°C which was continuously perfused with ACSF at 2 ml/min. Field excitatory postsynaptic potentials (fEPSPs) were recorded in CA1 stratum radiatum with glass electrodes (2–3 MΩ) filled with ACSF. Schaffer collateral fEPSPs were evoked with a concentric bipolar tungsten stimulating electrode placed in stratum radiatum proximal to CA3 region. Baseline stimulation was applied every 30 s (0.033 Hz) by delivering 0.1 ms pulses, with intensity adjusted to evoke 35% of maximal fEPSPs. For the induction of L-LTP, theta-burst stimulation (TBS, 15 bursts of four pulses at 100 Hz separated by 200 ms intervals) was performed. For analysis, the slope of the fEPSPs was measured and values were normalized to the averaged baseline slope value for each recording. Percentage of potentiation was calculated as the difference between averaged values for a 30-min period before the tetanus (baseline) and the last 10 min of recording.

Self-Grooming Test

Mice were placed in a new Plexiglas cage with fresh bedding and no nest or cardboard material, as previously described[15]. Self-grooming behaviour was recorded for 10 min after an initial 10 min habituation phase[15] at room light of 5 lux.

3-chamber Social Interaction Test

Sociability and social novelty were measured in a rectangular apparatus divided into 3 inter-connected chambers (each chamber: 36 x 28 x 30 cm, L x W x H). The test consisted of four sequential 10-min trials: (1) habituation to centre chamber, (2) habituation to all chambers, (3)

sociability, measured as the time the mouse spent in proximity to a conspecific or an object and (4) social novelty preference as measured by the time the mouse spent with an unfamiliar conspecific or a familiar one. The test was conducted at 5 lux. Behaviours were video recorded and the time exploring the cylinder was measured by a blind observer. Preference in exploration shown by the test mouse was assessed in % according to the formulas: t [mouse] / (t [mouse] + t [object]) and t [novel mouse] / (t [novel mouse] + t [familiar mouse]).

Synaptosome Preparation

Synaptosomes were prepared using the whole brain of adult (~3-month-old) WT (wild-type) or Mnk DKO male mice of each genotype using the Syn-PER™ Synaptic Protein Extraction Reagent (Thermo Fisher) as per the manufacturer's instructions. The lysis buffer was supplemented with 100 µg/ml cycloheximide for ribosome profiling (Sigma-Aldrich) and protease (Complete EDTA-free, Pierce) and phosphatase inhibitor (PhosSTOP, Sigma-Aldrich) tablets. Synaptosome lysates were stored at -80^{o}C until use.

Ribosome Profiling of Mouse Whole Brain and Synaptosomes

We used the Epicentre TruSeq Ribo Profile (Mammalian) Kit (Illumina, RPYSC12116), as previously described[9,14,16,17], with some modifications[9,14,16,17], to generate sequencing libraries. In brief, polysomes were extracted from snap-frozen, whole brain (from 1 animal) or synaptosomes (from 2-3 animals) of each genotype in the presence of cycloheximide. A portion of the lysate was used for footprint generation using TruSeq Ribo Profile Nuclease (Ribosome Protected Fragments, RPF), while an equal portion of the lysate was kept as an internal transcription control (Total mRNA). After digestion, RPFs corresponding to monosomes were size-purified on MicroSpin S-400 columns as described in the kit to enrich for small RNA fragments (28-32 nt). RPF and Total mRNA were depleted of ribosomal RNA using the Ribo-Zero Gold (Human/Mouse/Rat) Kit (Illumina, MRZG126). RPFs were further purified on a 15% TBE-Urea polyacrylamide gel, selecting bands running between 28 and 32 nt. Total mRNA samples were heat fragmented. All samples were end-repaired using TruSeq Ribo Profile Polynucleotide kinase, followed by ligation of a TruSeq Ribo Profile 3' Adapter. All samples were reverse

transcribed into cDNA, followed by a further PAGE purification on a 10% TBE-Urea gel, to separate sample cDNA from excess adapter. Purified cDNA was circularised, and PCR amplified, following purification using the Agencourt AMPure XP kit (Beckman Coulter). PCR products were further purified on an 8% TBE polycrylamide gel, to yield sufficient quantity and quality for sequencing. All samples were analysed on an Agilent Bioanalyzer High Sensitivity DNA chip to confirm expected size range and quantity and sequenced on an Illumina HiSeq 2500 system.

Bioinformatics Analysis

Data were analysed as previously described with modifications[9,14,16,17]. Synaptosome ribosome profiling analysis was carried out as described previously[17]. Sequencing data were de-multiplexed by the sequencing facility (Edinburgh Genomics). Obtained sequences were analysed using a custom developed pipeline (following the methods used by Ingolia *et al*[18]). In brief, reads were adapter-trimmed using the FASTX toolkit, contaminant sequences (rRNA, tRNA) removed using bowtie and reads aligned to a reference genome using STAR. Cufflinks was used to quantify reads and calculate RPKM values for each transcript. Translational efficiency for each transcript was calculated by dividing RPKM values of the RPF libraries by RPKM values of the Total mRNA libraries. Changes in transcription were analysed for pairwise comparisons, based on experimental design, using microarray normalization methods, as reviewed by Quackenbush[19]. Changes in translation were assessed using the R package Xtail v1.1.5[20].

GO Analysis

GO analysis was carried out, as previously[9,14,17], with Ingenuity Pathway Analysis [(IPA, Qiagen, Inc) Datasets were uploaded on IPA and submitted to Core Analysis with analysis parameters set to include Direct and Indirect Interactions and Experimentally Observed data only. Ingenuity Canonical Pathways were obtained for all datasets and processed according to p-value], or DAVID [(Database for Annotation, Visualization and Integrated Discovery, version 6.8). Datasets were submitted to DAVID and GO annotation gathered for KEGG pathways and

Molecular Function and Cellular Component Gene Ontology Annotations], or g:profiler software [Functional enrichment analysis was carried using the g:Ghost package of g:profiler to assign Gene Ontology categories to ribosome profiling lists of differentially translated genes[21]. Hierarchical filtering was used - best per parent group-strong. The probability threshold for all functional categories was set at 0.05, using correction for multiple testing with the g:SCS algorithm[21]]. All output from GO analyses is summarized in the respective Supplementary Figures and Tables.

Quantitative Proteomics and Phospho-Proteomics

Whole brain and synaptosome lysates were prepared as previously[14,17]. Four times the sample volume of cold (-20°C) acetone was added to the lysates in 1.5 ml Eppendorf tubes followed by vortexing for 10 sec and overnight incubation at -20°C. Next the samples were centrifuged at 15,000 × g at 4^{o}C for 10 minutes. The supernatant was removed and the uncapped tubes were kept at room temperature for 30 minutes to allow evaporation of remaining acetone. The resulting pellets were stored at -80^{o}C until analysis. For each sample, 500 µg of pellets of whole brain or synaptosome lysate (measured by Bradford assay) were reconstituted in 50 mM ammonium bicarbonate with 10 mM TCEP [Tris(2-carboxyethyl) phosphine hydrochloride; Thermo Fisher Scientific], and vortexed for 1 h at 37°C. Chloroacetamide (Sigma-Aldrich) was added for alkylation to a final concentration of 55 mM. Samples were vortexed for another hour at 37°C. 10 microgram of trypsin was added, and digestion was performed for 8 h at 37°C. Samples were dried down in a speed-vac. For the TiO_2 enrichment procedure, sample loading, washing, and elution were performed by spinning the microcolumn at 8,000 rpm at 4 °C in a regular Eppendorf microcentrifuge. The spinning time and speed were adjusted as a function of the elution rate. Phosphoproteome enrichment was performed with TiO_2 columns from GL Sciences. Digests were dissolved in 400 µL of 250 mM lactic acid (3% TFA/70% ACN) and centrifuged for 5 min at 13,000 rpm, and the soluble supernatant was loaded on the TiO2 microcolumn previously equilibrated with 100 µL of 3% TFA/70% ACN. Each microcolumn was washed with 100 µL of lactic acid solution followed by 200 µL of 3% TFA/70% ACN to remove nonspecific binding peptides. Phosphopeptides were eluted with 200 µL of 1% NH4OH pH 10 in water and acidified with 7 µL of TFA. T Eluates from TiO_2 microcolumns were

desalted using Oasis HLB cartridges by spinning at 1,200 rpm at 4 °C. After conditioning with 1 mL of 100% ACN/0.1% TFA and washing with 0.1% TFA in water, the sample was loaded, washed with 0.1% TFA in water, then eluted with 1 mL of 70% ACN (0.1% TFA) prior to evaporation on a SpeedVac. The extracted peptide samples were dried down and solubilized in 5% ACN-0.2% formic acid (FA). The samples were loaded on an Optimize Technologies C_{18} precolumn (0.3-mm inside diameter [i.d.] by 5 mm) connected directly to the switching valve. They were separated on a home-made reversed-phase column (150-µm i.d. by 150 mm) with a 240-min gradient from 10 to 30% ACN-0.2% FA and a 600-nl/min flow rate on a Nano-LC-Ultra-2D (Eksigent, Dublin, CA) connected to a Q-Exactive Plus (Thermo Fisher Scientific, San Jose, CA). Each full MS spectrum acquired at a resolution of 70,000 was followed by 12 tandem-MS (MS-MS) spectra on the most abundant multiply charged precursor ions. Tandem-MS experiments were performed using higher-energy collisional dissociation (HCD) at a collision energy of 25%. The data were processed using PEAKS 8.5 (Bioinformatics Solutions, Waterloo, ON) and a Uniprot mouse database. Mass tolerances on precursor and fragment ions were 10 ppm and 0.01 Da, respectively. Variable selected posttranslational modifications were carbamidomethyl (C), oxidation (M), deamidation (NQ), acetyl (N-term) and phosphorylation (STY). The data were visualized with Scaffold 4.3.0 (protein threshold, 99%, with at least 2 peptides identified and FDR<0.1% for peptides).

Co-Immunoprecipitation

Freshly dissected whole mouse brain samples were homogenized in lysis buffer (50 mM HEPES pH 7.4, 150 mM NaCl, 1% CHAPS + protease inhibitor + phosphatase inhibitor) on ice using a Dounce glass homogenizer. The homogenates were incubated for 20 min at 4^{o}C with rotation, followed by centrifugation at 15,000 rpm for 10 min at 4^{o}C. The collected supernatants were precleared with 50 µl of pre-washed protein A agarose slurry beads on rotator for 30 min at 4^{o}C followed by centrifugation at 3,500 rpm for 1 min at 4^{o}C to collect the precleared supernatant. The precleared supernatants were incubated with either 3 µg of normal rabbit IgG (CST #2729S) or 3 µg of Mnk1 antibody (CST #2195S) for 30 min at 4^{o}C, followed by incubation with 50 µl of pre-washed protein A agarose slurry beads overnight at 4^{o}C. The mixtures were centrifuged at 3,500 rpm for 1 min at 4^{o}C to remove the supernatant as unbound fraction. Beads were washed 3

times with lysis buffer for 10 min at 4°C and the bound proteins were eluted in 2x SDS sample buffer.

Analysis of IP proteomics

Mass spectrometry data was analyzed using MaxQuant v1.5.8.3 using the label free quantification (LFQ) settings and interactors were filtered in Perseus v1.5.8.5. Proteins were selected that contained at least one unique peptide and three valid values in triplicates of Mnk or IgG pull-down groups. Values were log2 transformed and missing values were replaced by random values that were drawn from normal distribution using the default settings (Width = 0.3, Down shift = 1.8) and as described previously[22]. Significance of fold changes was calculated using a 2-sided *t*-test and p-values were corrected for multiple testing using 250 permutation-based FDR correction. Interactors were defined significant when fold change was greater than the 99% confidence interval of IgG fold change ($log_2FC>3.5$) and FDR<0.05 (–Log FDR was greater than 1.3). Corresponding volcano plots were generated using R.

Phosphoserine IP

Whole brains were freshly dissected from wild-type mice (*Mnk1*$^{+/+}$*Mnk2*$^{+/+}$). The Synaptosomal fraction was prepared from one hemisphere as described above, while the other hemisphere was homogenised in lysis buffer (50 mM HEPES pH 7.4, 150 mM NaCl, 1% CHAPS + protease inhibitor + phosphatase inhibitor) on ice using Dounce glass homogenizer. The homogenates (whole brain or synaptosome) were rotated for 20 min at 4°C and centrifuged at 15,000 rpm for 10 min at 4°C, followed by collection of the supernatant, which were subsequently precleared with 50 µl of protein A agarose slurry beads for 30 min at 4°C. The mixtures were centrifuged at 3,500 rpm for 1 min at 4°C and the precleared supernatants were collected. The precleared supernatant (1.8 mg of whole brains, 600 µg of synaptosome fractions) were incubated with phosphoserine antibody (Millipore, AB1603) for 30 min at 4°C, followed by addition of and incubation with 50 µl of protein A agarose slurry beads at 4°C, overnight. The mixtures were subsequently centrifuged at 3,500 rpm for 1 min at 4°C. The first supernatants were collected as

unbound fractions. Beads were washed with lysis buffer 3 x 10 min, at 4°C and the bound proteins were eluted in 2x SDS sample buffer.

Plasmid generation (mutant Syngap1)

Mouse Syngap1 CDS (wild-type or S788A or S788D) were synthesised using Custom Gene Synthesis (Biomatik, Canada) and were subcloned to the pBSK(+) vector and subsequently transferred using blunt cloning to a pcDNA3.1(+) backbone (Addgene) to generate the final plasmids. Syngap1 sequence was confirmed with Sanger sequencing.

Mammalian cell culture and transfection

All cell culture and transfection reagents were from ThermoFisher Scientific. Human Embryonic Kidney cells (HEK-293H ATCC® CRL-1573) were cultured (37°C, 5% CO2) in Dulbecco's modified Eagle's medium (DMEM, 11995065) supplemented with 10% fetal bovine serum (10500064) and 1% Pen/Strep (15140148). Transient transfection was performed with Lipofectamine 3000 (L3000008) in Opti-MEM (31985070) following the manufacturer's protocol for 48 h.

SUrface SEnsing of Translation (SUnSET) assay

After 48h of transfection, cells were pulsed with 5 µg/mL puromycin hydrochloride for 1 h in culture medium. Cells were washed three times with ice cold PBS and lysed in RIPA buffer (10 mM Tris-HCl, pH 8.0, 1 mM EDTA, 0.5 mM EGTA, 1% Triton X-100, 0.1% Sodium Deoxycholate, 0.1% SDS, 140 mM NaCl; all from Sigma, supplemented with phosphatase and protease inhibitors; Roche) for immunoblotting with anti-puromycin antibody (MABE343; 12D10 Sigma). Puromycin incorporation was quantified with ImageJ (immunoblot signal intensity) and was normalised to control (no puromycin or no antibody) and membrane background signals.

Rheb GTPase and Syngap1 GAP activity assays

Rheb GTPase assay and Syngap1 GAP activity assays were performed according to the GTPase-Glo™ Assay manufacturer's instructions (Promega, V7681). Recombinant Rheb protein (0-2.5µg, Abcam, ab78768) was used in reactions containing 10µM GTP in GTPase/GAP Buffer and 1mM DTT. Reactions were incubated for 90 minutes at room temperature. For the Syngap1 GAP activity assay, immunoprecipitated Syngap1 from HEK-293H cells transfected with empty vector, wild-type, S788D or S788A Syngap1 was added to a Rheb GTPase reaction in GTPase/GAP Buffer containing 10µM GTP, and 1 µg Rheb (Abcam, ab78768). GTPase reactions for Syngap1 GAP activity were incubated for 2 hours. For both assays, GTPase-Glo™ Reagent was then added. After a further incubation of 30 minutes at room temperature Detection Reagent was added and luminescence was recorded on a PerkinElmer LS55 luminometer. Luminescence is measured as Relative light units (RLU) and corresponds to residual GTP amount after the GTPase reaction.

Syngap1 immunoprecipitation

500 µg of transfected HEK-293H lysate or mouse brain synaptosomes resuspended in RIPA buffer (20 mM Tris-HCl pH 7.5, 150 mM NaCl, 1 mM Na2EDTA, 1 mM EGTA, 1% NP-40, 1% sodium deoxycholate, 2.5 mM sodium pyrophosphate, 1 mM beta-glycerophosphate, 1 mM Na3VO4, 1 µg/ml leupeptin and 1mM PMSF) were incubated with 20 uL of protein G beads (Invitrogen, 10003D) preincubated with 1 µg rabbit IgG (Sigma, 12-370) or Syngap1 antibody (ThermoFisher Scientific, rabbit polyclonal, PA1-046) for 1h at 4 ^{o}C. Samples were washed thrice with RIPA buffer and either processed with immunoblotting or stored at -80 ^{0}C.

Active Rheb (Rheb-GTP) immunoprecipitation assay

Rheb-GTP was detected with immunoblotting using the Rheb Pull-Down Activation Assay Kit (New East Biosciences, 81201). Transfected HEK293-H cells were washed thrice with PBS and lysed in glass dounce homogenisers. Lysates were left on ice for 15 min with occasional vortexing and then centrifuged at 4^{o}C at 16,000 x *g* for 20 min. A total of 1mg of the supernatant was used to immunoprecipitate active-Rheb, to which 1 µg anti-Rheb-GTP antibody (New East Biosciences, Cat. # 26910) and 20 µL of A/G Agarose bead slurry (New East Biosciences, Cat. #

30301) were added. Samples were incubated for 1 hour at 4°C with gentle agitation. Beads were collected through centrifugation at 5,000 x g for 1 min, washed thrice with Assay/Lysis Buffer (New East Biosciences) and resuspended in SDS-PAGE buffer for immunoblotting.

Immunoblotting

Dissected brain tissue, HEK293-H lysates, immunoprecipitates, cap-column or synaptosomes were homogenized in RIPA (see above) or buffer B (50 mM MOPS/KOH pH 7.4, 100 mM NaCl, 50 mM NaF, 2 mM EDTA, 2 mM EGTA, 1% NP-40, 7 mM β-mercaptoethanol), both supplemented with protease and phosphatase inhibitors (Roche), using a glass Dounce homogenizer (~30 strokes). Samples were incubated on ice for 15 min, with occasional vortexing, and cleared by centrifugation for 20 min at 16,000 *g* at 4°C. The supernatant was used for western blotting after the protein concentration of each sample was determined by measuring A280 Absorbance on a NanoDrop (ThermoFisher Scientific). 50 µg of protein per lane were prepared in SDS Sample Buffer (50mM Tris pH 6.8, 100 mM DTT, 2% SDS, 10% Glycerol, 0.1% bromophenol blue), heated to 98°C for 5 min and resolved on 10-16% polyacrylamide gels. Proteins were transferred to 0.2 µm nitrocellulose membranes (Bio-Rad), blocked in 5% BSA in TBS-T (10 mM Tris pH 7.6, 150 mM NaCl, 0.1% Tween-20) for 1 h at RT, incubated with primary antibodies overnight at 4°C and with secondary antibodies for 1 h at RT. Primary antibodies were diluted in 1% BSA in TBS-T containing 0.02% Na azide, and between incubations membranes were washed extensively in TBS-T. Blots were imaged using an Odyssey Imaging System (Li-COR Biosciences) at a resolution of 169 µm and quantified using the ImageStudio Software (Li-COR Biosciences). For quantitative Western Blotting, the intensity of each protein band was measured in triplicate to minimize measuring variability. HSC70 or *β*-actin were used as a loading control. Data are shown as arbitrary units (AU) as a proxy for protein expression, after normalization to control (for protein phosphorylation: phospho-protein values were measured with Image J or Image Studio™ Lite and divided to total protein and to loading control: HSC70, *β*-actin or GAPDH band intensity values, after subtracting immunoblot background intensity).

AAV9-shRNA cloning and preparation

AAV9-shRNA viral particles were prepared by Vector Biolabs. The validated sequence targeting Syngap1 was: 5'-CACC-GCTCTATCAAACGTACAAAGTCTC-GAGACTTTGTACGTTTGATAGAGC-TTTTT-3' and the scrambled sequence used as control was: 5'-CACC-GAACAAGATGAAGAGCACCA-CTCGAG-TGGTGCTCTTCATCTTGTTC-TTTTTT-3'.

Intrahippocampal injection of AAV9

Four-week-old mice were anesthetised using isoflurane and secured in the stereotaxic apparatus (Kopf). A midline incision was made to expose the skull and two holes were drilled above the CA1 region of the hippocampi (AP: - 1.90 mm, ML: ± 1.0 mm, and DV: - 1.50 mm). Next, 1 µl of either AAV9-GFP-U6-scramble-shRNA (3.1 x 10E13 GC/ml) or AAV9-GFP-U6-mSyngap1-shRNA (1.3 x 10E13 GC/mL) were bilaterally injected into the CA1 using a 10 µl Hamilton syringe connected to a 23-gauge needle mounted on a perfusion pump (Harvard Apparatus, pump 11 Elite). Injection rate was set at 500 nL per minute and the needle was left for 3 additional minutes before it was slowly withdrawn.

eFT508 treatment

eFT508 (MCE, New Jersey, USA), which was dissolved as concentration stocks (3.22 mg/mL) in Tween 80 (20% v/v), DMSO (32% v/v) and PBS (48% v/v) were freshly diluted in PBS to appropriate working concentrations (1 mg/mL). Intraperitoneal injections (1 mg/kg) were carried out daily for 5 days prior to behavioural tests and throughout the experiment. Behavioural tests were performed 24 h after the last injection.

Statistical Analysis

Experimenters were blinded to the genotype during testing and scoring for all behavioural tests in this study and for all molecular and bioinformatics analysis. All data are presented as mean ± S.E.M. (error bars) and individual experimental points are depicted in column or bar graphs. No nested data were obtained in this study, as we only collected one observation per research object. Exclusion criteria for animal experimentation included only poor health as assessed by trained

veterinarians and a routine overall health assessment during colony monitoring. Statistical significance was set *a priori* at 0.05 (n.s.: non-significant). No randomization was performed in the design and implementation of this study. Sample size was determined using power analysis only for rodent behavioural experiments and was based either on published or pilot data using G*Power (80% power and 0.05 alpha). Details for statistical tests used were provided within figure legends or the relative methods description and summarized in Supplementary Table 9. Statistical analysis was carried out using Graphpad Prism 9.

Data availability

RNA-seq and proteomics data (~70 GB and description) are available from the authors upon reasonable request. Proteomics data are available at Mendeley Data, V1, doi: 10.17632/6mssjkcjz2.1

Results

Mnk1/2 depletion impairs synaptic plasticity, learning and memory

We previously showed that *Eif4e*^{Ser209Ala} mice display intact hippocampal synaptic plasticity, learning and memory[9]. Unlike *Eif4e*^{Ser209Ala} mice, Mnk DKO mice exhibited impaired spatial learning and memory in the Morris water maze test (Fig. 1a) and showed significantly decreased long-term memory in the contextual fear conditioning test 24 h after training (~31% reduction in freezing behaviour in Mnk DKO, Fig. 1b). In addition, we examined social behaviour (social approach and preference for social novelty) and we did not detect any significant changes between Mnk DKO and wild type mice (Fig. 1c). Self-grooming was significantly increased in Mnk DKO mice (total time grooming, but not the number of grooming bouts (Fig. 1 c,d). Moreover, the late phase of LTP (L-LTP) in CA1 hippocampal area, a form of plasticity which is MAPK- and protein synthesis-dependent[23,24], was impaired in Mnk DKO mice. Theta-burst stimulation (TBS) of the Schaffer collateral-CA1 synapses elicited long-lasting potentiation of field excitatory post-synaptic potentials (fEPSPs) in wild-type, but not in Mnk DKO hippocampal slices (Fig. 1c, d). Taken together, these data show that Mnk1/2 deletion impairs L-LTP and hippocampus-dependent learning and long-term memory.

Altered translational landscape in Mnk1/2 DKO brain

Given the cardinal role of Mnk kinases in translational control, and the significant effects of their deletion on behaviour (Fig. 1), we measured the genome-wide changes in mRNA translation in Mnk DKO mice using ribosome profiling[25]. Using whole brain tissue, we generated libraries for RNA sequencing from fragmented poly(A)-enriched total RNA (to measure mRNA abundance) and from ribosome-protected footprints following RNase I digestion (to measure translation), to assess the genome-wide translation efficiency (TE) of mRNAs (Fig. 2a). Ribosome profiling yielded high-quality reads, as shown by the high correlation in Reads Per Kilobase of transcript per Million mapped reads (RPKM) between biological replicates (R^2 < 0.95), the canonical distribution of footprint size (28-32 nt), the read distribution within the 3 mRNA reading frames and by the canonical periodicity of ribosomal footprints across mRNA's coding and non-coding regions (Supplementary Fig. 1a, b, c, d). We observed a modest reduction in global translation (~17.2%) and no significant change in global mRNA levels in Mnk DKO whole brain (Fig. 2b; R^2 0.828 and 0.993, respectively). However, we detected significant changes in translation efficiency and abundance of specific mRNAs. Differentially translated genes (DTGs) in Mnk DKO included 51 upregulated and 57 downregulated mRNAs, while differentially expressed genes (DEGs) included 55 upregulated and 134 downregulated genes (False Discovery Rate [FDR] < 15% for DTG and < 10% for DEG; Fig. 2b). Gene ontology (GO) analysis revealed extracellular matrix (ECM) as a major category significantly enriched in Mnk DKO DTGs and DEGs, while other categories include calcium ion binding, circadian rhythm and links to neurological disorders, cancer, and embryonic development (Supplementary Fig. 1e, f and Supplementary Table 1, 2). Interestingly, comparison of Mnk DKO whole brain ribosome profiling to *Eif4e*^{Ser209Ala} (carried out previously in[9]) revealed only 20 common DTGs (Fig. 2c), 19 common DEGs (Supplementary Fig. 2a) and a very low correlation between these datasets (R^2 = 0.048). The top GO categories for the 20 common DTGs are related to ECM (Fig. 2c). While this result is in accordance with previous studies[7,26], and further highlights a key role for translational control via eIF4E Ser209 phosphorylation downstream of Mnks in the regulation of ECM, it also suggests that there are other yet unidentified Mnk1/2 downstream targets underlying Mnk1/2-mediated translational regulation in the brain.

Mnk1/2 deletion remodels whole brain and synaptic phosphoproteome and alters synaptic translation

To study the molecular substrates of Mnk kinases in the brain, we carried out label-free phospho-proteomics mass-spec (MS) analysis of wild-type and Mnk DKO mice whole brain lysates using Titanium Dioxide (TiO_2) mediated selective enrichment of phosphorylated peptides, coupled with liquid chromatography–mass spectrometry (LC–MS). Whole brain phosphoproteomic analysis revealed significant changes in a sizable portion of phosphopeptides in Mnk DKO brains compared with wild-type (fold change > 2, *p*-value < 0.05; 145 downregulated and 164 upregulated unique phosphopeptides) (Fig. 3a and Supplementary Table 3). Motif analysis of the downregulated phosphopeptides in Mnk DKO whole brain, using the motif-x biological sequence motif discovery tool[27], revealed a ~ 24-fold enrichment for the motif RxxSxSP (Fig. 3b). Interestingly, more than 70% of the differentially phosphorylated proteins in Mnk DKO whole brains are annotated as synaptic proteins or linked to synaptic function and the GO analysis revealed several significantly regulated categories, with an enrichment for synaptic compartments (postsynaptic density, synapse, dendrite), which are also linked to local protein synthesis (Fig. 3c and Supplementary Table 4). Notably, predicted upstream regulators include Ca^{2+} and the Cyclin-dependent kinase 5 (CDK5) and its activator enzyme CDK5R1 (Fig. 3d and Supplementary Table 4).

Because of the enrichment of synapse-related GO categories in whole brain Mnk DKO lysates, suggesting a potential mechanistic link between the changes in synaptic phosphoproteome and the role of Mnks in brain, we performed phosphoproteomics on synaptosome fractions (Fig. 3e). We extracted synaptosomal fractions with high purity, as evidenced by enrichment for pre- and post-synaptic proteins and depletion of nuclear markers and glial-specific proteins (Supplementary Fig. 3). Mnk1/2 deletion induced pervasive changes in the synaptic phosphoproteome, even more so when compared with whole brain (Fig. 3e). We found 469 downregulated and 423 upregulated unique phosphopeptides in Mnk DKO brains compared with wild-type (fold change > 2, *p*-value < 0.05; Fig. 3e and Supplementary Table 3). Compared to whole brain, motif-x analysis identified a similar, albeit better-defined phosphorylation motif: SP*E*KSP*EAK (hereafter referred to as “SPEAK” motif), with 166.97-fold enrichment among

downregulated synaptic phosphopeptides in Mnk DKO (Fig. 3f). The SPEAK motif is similar to phosphorylation motifs of other kinases: Glycogen synthase kinase-3 (GSK3)[28], CDK5[29] and ERK[30] (Supplementary Fig. 4a). Akin to whole brain phosphoproteomics, postsynaptic density and Ca^{2+} transport were among the top GO categories (Fig. 3g and Supplementary Table 4), while Ca^{2+}, CDK5 and CDK5R1 were the top upstream regulators (Fig. 3h and Supplementary Table 4). In particular, for the diseases and functions category of the IPA analysis, the synaptosomes phosphoproteomics dataset contained significantly more proteins within the Nervous System Development and Function and Behaviour categories, compared with the whole brain dataset (Fig. 3i and Supplementary Table 4). Given the spatial memory phenotypes in Mnk DKO mice (Fig. 1) and the emerging role of Mnks in ASD, we compared the phosphoproteomics datasets to Simons Foundation Autism Research Initiative (SFARI) syndromic genes and FMRP CLIP mRNAs[31,32] and identified several common targets (Supplementary Fig. 5a), while there is also a significant overlap between our datasets and a previous SILAC proteomics dataset from Mnk1 mouse knockout neurons[6] (Supplementary Fig. 5b). Finally, it is plausible that the SPEAK motif is not a *bona fide* Mnk1/2 phosphorylation motif, but its enrichment is the result of indirect phosphorylation by other kinases. Thus, we identified known kinases, which were differentially phosphorylated in the whole brain and synaptosome datasets, among which is Calcium/Calmodulin Dependent Protein Kinase II Alpha (CamKIIα) (Supplementary Fig. 4b, c). Several phosphorylation sites corresponding to CamKIIα are among the top differentially phosphorylated (upregulated and downregulated) in Mnk DKO whole brain and synaptosomes (Supplementary Table 3). Pathway analysis of known kinases identified in Mnk DKO whole brain and synaptosomes phosphoproteomics datasets highlighted several significantly altered categories, such as inositol triphosphate (IP3) and diacylglycerol (DAG) pathway, inflammation (TRP channels), LTP, insulin resistance, calcium and calmodulin related pathways and α-amino-3-hydroxy-5-methyl-4-isoxazolepropionate (AMPA) receptor trafficking (Supplementary Fig. 4b, c). We also detected oxytocin signalling among GO categories (Supplementary Fig. 4c) in accordance with a recent report[8].

Because of the pronounced effects of Mnk1/2 deletion on the synaptic phosphoproteome, we reasoned that local mRNA translation could also be significantly affected. To this end, we employed ribosome profiling in synaptosomes, a technique recently developed in our lab[17] (Fig.

4a). We generated high quality ribosome profiling libraries from synaptosomes (Supplementary Fig. 2b, c, d, e, f) and detected 122 DTG in Mnk DKO (Fig. 4a and Supplementary Table 5). We detected a modest correlation between Mnk DO whole brain and synaptosome translational efficiency (R^2 = 0.689) (Fig. 4b), suggesting that the translation of a distinct subset of synaptic mRNAs is regulated by Mnk1/2. ~10% of mRNAs that are downregulated in Mnk1/2 DKO synaptosome were also downregulated in Mnk1/2 DKO brain (Supplementary Fig. 5c, d). GO analysis of Mnk1/2 translationally controlled mRNAs in synaptosomes revealed enrichment for mitochondria related categories, but on ECM-related genes (Supplementary Table 6). Furthermore, several ribosomal protein coding mRNAs were also translationally downregulated in Mnk DKO (Supplementary Table 5), consistent with an mTORC1 downregulated signature in Mnk DKO brain (see below) (see also ref.[33]). Together, these data reveal a pivotal role for Mnk1/2 kinases in the regulation of the synaptic phosphoproteome and synaptic mRNA translation, with wider implications for synaptic plasticity, learning, memory, and autism-related behaviours.

Mnk binds to and modulates Syngap1 phosphorylation

Mnk1 is the predominant Mnk in the brain[6]. To identify targets that may directly bind to and are phosphorylated by Mnks, we performed an immunoprecipitation assay using the Mnk1 antibody in whole brain lysates (Supplementary Fig. 6a). We detected in immunoprecipitates a single band of ~48 kDa corresponding to Mnk1, evident by Coomassie blue stain and confirmed by immunoblotting with Mnk1-specific antisera, which was absent from Immunoglobulin G (IgG) control (Supplementary Fig. 6b). Quantitative mass-spectrometric analysis detected Mnk1 along with 10 other proteins as the top targets among the immunoprecipitated proteins ($\log_2$ fold change > 3.5, FDR < 0.05, Fig. 5a and Supplementary Table 7). Interestingly, the only common target between the Mnk1 interactors and the differentially phosphorylated proteins in the Mnk DKO mice was Syngap1 (Fig. 5a), which is linked to intellectual disability and is a syndromic ASD gene[34]. We confirmed the Mnk-regulated phosphorylation of Syngap1 by immunoprecipitation with anti-phosphoserine antibody in wild-type and Mnk DKO brain lysates and immunoblotting with the Syngap1 antibody, which revealed significantly reduced levels of phosphorylated Syngap1 in Mnk DKO compared with WT brain lysates (~65% decrease; Fig.

5b). In our phosphoproteomics dataset, we detected two phosphorylation sites on Syngap1: S788 (downregulated in Mnk DKO) and S1165 (upregulated in Mnk DKO), which are highly conserved between mouse, rat and human (Fig. 5c). Intriguingly, these sites are proximal to known CDK5 and CamKIIα phosphorylation sites on rat Syngap1[35] (Fig. 5c, bottom). Recent analysis of several human Syngap1 variants[36] and previous work[35] showed that CDK5 phosphorylates Syngap1 at S788.

Given previous research linking Syngap1 to regulation of protein synthesis[11,13], we reasoned that phosphorylated Syngap1 S788 could constitute a newly identified effector of Mnk1 in brain, regulating translation and ultimately synaptic plasticity, memory, and autism-like behaviours. To assess the role of the Syngap1 S788 phospho-site in regulation of global protein synthesis, we generated Syngap1 wild-type and phospho-mutant (*Syngap1*^{S788A}; phospho-mutant or *Syngap1*^{S788D} phospho-mimetic) expression constructs and performed transient transfection in HEK-293H cells (Fig. 5d). We then pulsed HEK-293H cells with puromycin and detected its incorporation into nascent peptides with immunoblotting (SUnSET method) (Fig. 5d). Expression of wild-type Syngap1 led to a ~30% decrease in puromycin incorporation (a proxy for global protein synthesis), compared with empty vector (Fig. 5d). Phospho-mimetic *Syngap1*^{S788D} expression displayed loss of function in inhibiting protein synthesis, while phospho-mutant *Syngap1*^{S788A} expression inhibited protein synthesis akin to wild-type Syngap1 (Fig. 5d). These data, in conjunction with the reduction in Syngap1 S788 phosphorylation in Mnk DKO brain (Fig. 3 & Supplementary Table 3), suggest that Mnk phosphorylation of Syngap1 on S788 promotes protein synthesis.

To further understand the link between Mnk1 and Syngap1, and because Syngap1 is known to regulate signalling pathways upstream of translation (*e.g.*, upregulation of mTORC1 signalling in *Syngap1*$^{+/-}$ mouse brain[13]), we examined three key pathways linked to translational control (mTORC1, Akt and MAPK) in synaptosomes from Mnk DKO and wild-type mice by immunoblotting for phospho-ribosomal protein S6 (rpS6 240/244 and 235/236 sites), phospho-Akt(S473) and phospho-ERK (T202/Y204), respectively (Supplementary Fig. 6c, d). We detected significantly decreased phosphorylation of rpS6 on both sites (240/244, 235/236) in Mnk DKO compared with wild-type, indicating decreased mTORC1 activity (Fig. 5e). We did not detect any significant changes in Akt or MAPK signalling (Supplementary Fig. 6c, d). Akt and Erk are downstream to Ras, which is regulated by Syngap1[37]. Thus, we reasoned that

plausibly Syngap1 S788 phosphorylation may regulate mTORC1 via increased GAP-activity for the Rheb GTPase, independent of p-ERK or p-Akt. To examine if S788 phosphorylation alters Syngap1 GAP activity towards Rheb GTPase (Supplementary Fig. 7a) we performed GAP activity assay using immunoprecipitated (IP) Syngap1 from HEK-293H cells (Supplementary Fig. 7b) transfected with the different mutants of Syngap1, using a recombinant Rheb GTPase assay based on luminescence (Fig. 5f). WT and S788A Syngap1 showed a significant increase in GAP activity for Rheb compared with empty vector, as evidenced by the decreased (~41%) residual GTP using recombinant Rheb in the GAP activity assay, compared with S788D (Fig. 5f). IgG immunoprecipitation control samples did not significantly affect Syngap1 GAP activity for Rheb (Supplementary Fig. 7c). To further elaborate on these findings, we performed active-Rheb (Rheb-GTP) immunoprecipitation from HEK293 cells transfected with the different mutants of Syngap1 (Fig. 5g). Wild-type and S788A expression led to reduced active Rheb (Rheb-GTP) recovered in the IP (Fig. 5g). We also detected decreased (~30.6%) residual GTP in Syngap1 immunoprecipitated from Mnk1/2 DKO brain synaptosomes compared with wild-type (Fig. 5h), indicating that immunoprecipitated Syngap1 has increased GAP activity for Rheb and that Rheb is significantly less active in Mnk DKO compared with wild-type mouse brain synaptosomes. IgG immunoprecipitation control samples did not significantly affect Syngap1 GAP activity for Rheb (Sup. Fig. 7d).

These data suggest that Mnk-mediated phosphorylation of Syngap1 promotes mTORC1 activity and thereby protein synthesis, possibly via reduced Syngap1 GAP-activity for Rheb-GTPase.

Syngap1 inhibition reverses memory deficits in Mnk DKO mice

To further characterise the physiological significance of the identified link between Mnk1 and Syngap1, we investigated whether increased Syngap1 activity in Mnk DKO mice underlies memory deficits in these animals. To this end, we generated adeno-associated virus 9 (AAV9) expressing short-hairpin RNAs (shRNAs) against mouse *Syngap1* mRNA, driven by the U6 promoter (AAV9-Syngap1-shRNA, Fig. 6a). We injected AAV9-Syngap1-shRNA or an AAV9 expressing scrambled sequence into the hippocampus of wild-type and Mnk DKO mice (Fig. 6a). AAV9-Syngap1-shRNA significantly decreased Syngap1 expression (~50%; Fig. 6a) 2 and 4 weeks post-injection. We then subjected 8-week-old wild-type and Mnk DKO to the Morris

water maze and contextual fear conditioning tests. Remarkably, decreasing Syngap1 expression with AAV9-Syngap1-shRNA completely reversed the spatial memory impairment (Fig.6a and Supplementary Fig.8a, b) and contextual fear memory deficits in Mnk DKO mice, without affecting wild-type animal behaviour (Fig. 6a). This result indicates that dysregulated (increased) Syngap1 expression and thus activity downstream of Mnk, underlies memory deficits in Mnk DKO mice.

Pharmacological inhibition of Mnk with eFT508 corrects behavioural phenotypes in *Syngap1*$^{+/-}$ mice

Pharmacological modulation of Mnks has recently emerged as a promising therapeutic avenue in cancer treatment[38], autism spectrum disorders[7,8], depression[9] and neuropathic pain[39]. Tomivosertib (eFT508) is a brain-permeable, highly specific inhibitor of Mnks[40]. Since Mnk-mediated phosphorylation suppresses Syngap1 activity, we hypothesised that inhibition of Mnk might increase Syngap1 activity, restore mTORC1 signalling and thus rescue behavioural deficits in *Syngap1*$^{+/-}$ mice. Thus, we injected Syngap1$^{+/-}$ mice intraperitoneally with 1 mg/kg eFT08 daily for 5 consecutive days, a regimen that effectively reduces Mnk activity in vivo[39] (Fig. 6b and Supplementary Fig. 7e). Syngap1$^{+/-}$ mice exhibit key autism-like phenotypes such as stereotypic behaviour, hyperactivity, and social behaviour deficits[41]. First, we subjected *Syngap1*$^{+/-}$ mice to a self-grooming test, where they displayed increased overall grooming time (Fig. 6b). Chronic eFT508 treatment completely reversed enhanced grooming in *Syngap1*$^{+/-}$ mice, while it did not affect grooming behaviour in wild-type animals (Fig. 6b). Second, in the open-field test, vehicle-treated *Syngap1*$^{+/-}$ mice spent significantly more time in the centre compared with wild-type, which is likely due to their hyperactivity (Fig. 6b). eFT508 treatment reversed the open-field phenotype of *Syngap1*$^{+/-}$ mice, without affecting wild-type animals (Fig. 6b). Third, we carried out social behaviour analysis in eFT508-treated *Syngap1*$^{+/-}$ mice using the 3-chamber social interaction and preference for social novelty tests (Fig. 6b). Vehicle-treated *Syngap1*$^{+/-}$ mice display impaired preference for social novelty but not sociability (Fig. 6b). eFT508 chronic treatment selectively rescued the preference for social novelty in *Syngap1*$^{+/-}$ mice, without affecting wild-type mice behaviour (Fig. 6b).

Importantly, both AAV9-shRNA-mediated Syngap1 inhibition and chronic eFT508 treatment normalised mTORC1 signalling in both mouse models. In Mnk DKO mice, shRNA against Syngap1 but not scrambled-shRNA restored reduced phosphorylation of rpS6 (240/244), suggesting that mTORC1 activity was normalised to wild-type levels (Fig. 6c). In *Syngap1*$^{+/-}$ mice, Mnk inhibition via chronic eFT508 treatment reduced enhanced phosphorylation of rpS6 (240/244) to wild-type levels (Fig. 6e). Altogether, pharmacological inhibition of Mnk kinase activity in *Syngap1*$^{+/-}$ mice with eFT508 normalised exaggerated mTORC1 signalling in *Syngap1*$^{+/-}$ mice, and reversed autism-related behaviours. These data further validate the mechanistic link between Mnks, Syngap1, and mTORC1 and highlight its importance at the behavioural level (Fig. 6d, f).

Discussion

While there is extensive and definitive evidence that Mnk kinases regulate the phosphorylation and activity of proteins involved in diverse cellular functions, only a few substrates of Mnks have been identified in the brain, where their roles remain elusive. Accordingly, phosphorylation of eIF4E on Ser209 by Mnks can partially account for the plethora of Mnks-regulated functions in the brain. Our work reveals a hitherto unknown link between Mnk kinases and the genetic ASD risk factor Syngap1 in regulating mTORC1 signalling and protein synthesis. Pharmacological and AAV-mediated knockdown experiments further reveal that the Mnk-Syngap1 axis is crucial for ASD-linked behaviours (such as social interaction), learning, and memory.

Translational control by the MAPK pathway is required for hippocampal synaptic plasticity, learning and memory[4], thus, it was surprising that *Eif4e*^{Ser209Ala} mice exhibit intact hippocampal learning and memory, as well as L-LTP[9]. Contrary to these findings, Mnk1/2 deletion in mice impairs learning and memory, and synaptic plasticity (Fig. 1). Furthermore, pharmacological inhibition of Mnk1/2 reversed social behaviour deficits in *Syngap1*$^{+/-}$ mice (Fig. 6) and restored social novelty in *Nlgn3* KO mice[8]. Taken together, our study highlights the role of Mnks in neurodevelopmental disorders such as ASD.

The common denominator between Mnks and syndromic ASD (Syngap1 or Ngn3) and FXS is translational control. Herein, we showed that Mnk1/2 deletion in mice remodels whole brain and synaptic translatome and phosphoproteome (Figs. 2, 3, 4). Importantly, there is a small overlap between Mnk DKO and *Eif4e*^{Ser209Ala} brain translatomes, chiefly comprised of ECM-related genes. While this is in accordance with the importance of translational control of ECM genes in neurodevelopmental disorders such as FXS[7,42], it further supports the notion that phosphorylation of eIF4E can only explain some aspects of Mnks in regulating brain functions. Interestingly, we detected pervasive changes in the synaptic translatome in Mnk DKO mice (Fig. 4), revealing a role for Mnks in regulating local translation, with wider implications for various synaptopathies. This finding may also be relevant to the emerging role for Mnks and eIF4E in depression via translational control of subsets of mRNAs[9,43].

We also observed significant remodelling of the synaptic phosphoproteome, whereby 892 phosphopeptides were differentially expressed in Mnk DKO (Fig. 3). In addition, we identified a consensus motif ("SPEAK") for Mnks, which is highly enriched in synaptic phosphoproteomics (Fig. 3). Because this motif is similar to motifs of other kinases (ERK, CDK5), it is plausible that Mnks may work in synergy with other kinases to phosphorylate a given subset of proteins. Such candidate kinases include CamKIIα and Cdk5, which are known to phosphorylate Syngap1[35]. Conceivably, Mnks could phosphorylate Syngap1 directly or in complex with CamKIIα/Cdk5, recruiting and phosphorylating Syngap1 on S788 (CamKIIα site) and S1165 (Cdk5 site). This is reminiscent of the mechanism by which Mnks phosphorylate eIF4E on Ser209, requiring first binding to eIF4G[44]. Mnk1 binding to Syngap1 (Fig. 5) at synaptic sites could lead directly or indirectly (via Cdk5/CamKIIα) to S788 phosphorylation, thus regulating local translation. Furthermore, expression of phosphor-mimetic Syngap1^{S788D} displays loss of function in inhibiting protein synthesis compared with wild-type Syngap1 (Fig. 5d). This suggests that Syngap1 S788 phosphorylation by Mnks is required to stimulate protein synthesis. In addition, we observed that mTORC1 is downregulated in Mnk DKO mice (Figs. 5, 6 and refs[11,13]), while Akt and Erk phosphorylation was not altered (Supplementary Fig. 6). Syngap1 displays GAP activity for several small GTPases upstream of Akt, Erk mTOR. (e.g., Ras). In S788 phosphomutant lysates (but not phosphomimetic) and in Mnk DKO synaptosomes (where S788 phosphorylation was reduced) we measured increased Syngap1 GAP activity for Rheb, leading to inhibition of active Rheb (Fig. 5f, g, h). As Rheb is an upstream mTORC1 activator[45],

collectively these findings may explain reduced mTORC1 signalling in Mnk DKO, concomitant with reduced Syngap1 S788 phosphorylation. p-Akt and p-ERK could remain unaltered in Mnk DKO due to homeostatic regulation of different phosphosites on Syngap1. Undoubtedly, Syngap1 phosphosites work in synergy, engendering complex output to its downstream effectors (e.g., ERK and mTORC1 kinases)[37], thus it will be interesting to systematically study the Syngap1 S788 phosphosite, in conjunction with Mnk1 in this signalling pathway.

mTORC1 signalling was previously linked to translational control of mitochondrial and ribosomal protein-coding mRNAs[33,46], which was recapitulated in our ribosome profiling in Mnk DKO (Fig. 2 and 4). mTORC1 and Mnks were implicated in neuropathic pain, via Ras-Related GTP-Binding Protein A (RagA)[33] and in cancer cells, via Phosphatidyl Inositol 3′ Kinase-related Kinase (PIKK) stabiliser Telomere Maintenance 2 TELO2[47]. Notably, dual abrogation of Mnk/mTOR emerges as a promising therapeutic avenue for aggressive cancers[48].

Furthermore, we reveal that in addition to eIF4E, Mnks have additional downstream effectors in a "context-dependent manner", which regulate mRNA translation. Plausibly, in synaptic sites, Mnk interaction with Syngap1 may exert local translational control via Syngap1/Rheb/mTORC1 pathway. Whereas in other sites Mnk1-mediated phosphorylation of eIF4E on Ser209 could have a more prominent, yet mTORC1-independent effect on the translatome. Moreover, Mnk1 via eIF4E, Syngap1, or other as yet unknown mediators may have divergent effects on mRNA translation in different brain regions and thus regulate different behaviours (e.g. memory, affective behaviours).

In Syngap1 animal and cellular models, mTORC1 was implicated in regulating protein synthesis in excitatory cortical neurons via AMPA receptors[11,13]. This previous work, in conjunction with our rescue experiments performed in Mnk DKO and *Syngap1*$^{+/-}$ mice (AAV knockdown and pharmacological inhibition, Fig. 6) further strengthens the Mnk-Syngap1 link to mTORC1 and protein synthesis. Our finding that eFT508 rescued autism-related behaviours in *Syngap1*$^{+/-}$ mice, harbouring only one functional allele of Syngap1, presents an appealing therapeutic avenue for this genetic condition. All SYNGAP1 mutations (e.g. *de novo*, rare variants) linked to ASD are loss-of-function and cause SYNGAP1 haploinsufficiency leading to a defined intellectual disability and epilepsy phenotype, termed Mental Retardation-type 5 (MRD5, OMIM #612621)[49]. Additionally, Mnk inhibitors could be used to reduce SYNGAP1 S788

phosphorylation in syndromic (e.g., FXS, Tuberous Sclerosis)[50] or sporadic ASD[51] associated with enhanced mTORC1 activity or protein synthesis.

In conclusion, by defining the Mnk phosphoproteome and translatome in whole brain and synaptosomes of Mnk DKO transgenic mice, we revealed a mechanistic link between Mnk and the syndromic autism risk protein Syngap1 (Fig. 7). This constitutes a previously unidentified mechanism of translational control in brain downstream of MAPK, with wider implications for synaptic plasticity, learning, memory, and autism-related behaviours.

Acknowledgements

We thank R. Fukunaga for the permission to use Mnk1/2 DKO mice and N. Sonenberg for providing the animals. We thank P. Kind and S. Grant for Syngap1 mice and W. Sossin for critical reading of the manuscript.

Funding

This work was supported by grants to C.G.G.: Start-up funds from the Foundation for Research and Technology, the Hellenic Foundation for Research and Innovation (H.F.R.I.) under the "2nd Call for H.F.R.I. Research Projects to support Faculty Members & Researchers" (Project Number: 2556), Sir Henry Dale Fellowship from the Wellcome Trust and Royal Society (107687/Z/15/Z), a NARSAD Young Investigator grant from the Brain & Behavior Research Foundation (24968). SMJ is supported by a Patrick G. Johnston Research Fellowship at Queen's University Belfast.

Competing interests

The authors report no competing interests.

Supplementary material

Supplementary material is available at *Brain* online.

References

1. Wang X, Flynn A, Waskiewicz AJ, et al. The phosphorylation of eukaryotic initiation factor eIF4E in response to phorbol esters, cell stresses, and cytokines is mediated by distinct MAP kinase pathways. J Biol Chem. Apr 17 1998;273(16):9373-7. doi:10.1074/jbc.273.16.9373

2. Sonenberg N, Hinnebusch AG. Regulation of translation initiation in eukaryotes: mechanisms and biological targets. Cell. Feb 20 2009;136(4):731-45. doi:10.1016/j.cell.2009.01.042

3. Joshi S, Platanias LC. Mnk kinase pathway: Cellular functions and biological outcomes. World J Biol Chem. Aug 26 2014;5(3):321-33. doi:10.4331/wjbc.v5.i3.321

4. Kelleher RJ, 3rd, Govindarajan A, Jung HY, Kang H, Tonegawa S. Translational control by MAPK signaling in long-term synaptic plasticity and memory. Cell. Feb 6 2004;116(3):467-79. doi:10.1016/s0092-8674(04)00115-1

5. Panja D, Kenney JW, D'Andrea L, et al. Two-stage translational control of dentate gyrus LTP consolidation is mediated by sustained BDNF-TrkB signaling to MNK. Cell Rep. Nov 20 2014;9(4):1430-45. doi:10.1016/j.celrep.2014.10.016

6. Genheden M, Kenney JW, Johnston HE, Manousopoulou A, Garbis SD, Proud CG. BDNF stimulation of protein synthesis in cortical neurons requires the MAP kinase-interacting kinase MNK1. J Neurosci. Jan 21 2015;35(3):972-84. doi:10.1523/JNEUROSCI.2641-14.2015

7. Gkogkas CG, Khoutorsky A, Cao R, et al. Pharmacogenetic inhibition of eIF4E-dependent Mmp9 mRNA translation reverses fragile X syndrome-like phenotypes. Cell Rep. Dec 11 2014;9(5):1742-1755. doi:10.1016/j.celrep.2014.10.064

8. Hornberg H, Perez-Garci E, Schreiner D, et al. Rescue of oxytocin response and social behaviour in a mouse model of autism. Nature. Aug 2020;584(7820):252-256. doi:10.1038/s41586-020-2563-7

9. Amorim IS, Kedia S, Kouloulia S, et al. Loss of eIF4E Phosphorylation Engenders Depression-like Behaviors via Selective mRNA Translation. J Neurosci. Feb 21 2018;38(8):2118-2133. doi:10.1523/JNEUROSCI.2673-17.2018

10. Ueda T, Watanabe-Fukunaga R, Fukuyama H, Nagata S, Fukunaga R. Mnk2 and Mnk1 are essential for constitutive and inducible phosphorylation of eukaryotic initiation factor 4E but not for cell growth or development. Mol Cell Biol. Aug 2004;24(15):6539-49. doi:10.1128/MCB.24.15.6539-6549.2004

11. Barnes SA, Wijetunge LS, Jackson AD, et al. Convergence of Hippocampal Pathophysiology in Syngap+/- and Fmr1-/y Mice. J Neurosci. Nov 11 2015;35(45):15073-81. doi:10.1523/JNEUROSCI.1087-15.2015

12. Nakajima R, Takao K, Hattori S, et al. Comprehensive behavioral analysis of heterozygous Syngap1 knockout mice. Neuropsychopharmacol Rep. Sep 2019;39(3):223-237. doi:10.1002/npr2.12073

13. Wang CC, Held RG, Hall BJ. SynGAP regulates protein synthesis and homeostatic synaptic plasticity in developing cortical networks. PLoS One. 2013;8(12):e83941. doi:10.1371/journal.pone.0083941

14. Simbriger K, Amorim IS, Lach G, et al. Uncovering memory-related gene expression in contextual fear conditioning using ribosome profiling. Prog Neurobiol. Aug 26 2020:101903. doi:10.1016/j.pneurobio.2020.101903

15. Gkogkas CG, Khoutorsky A, Ran I, et al. Autism-related deficits via dysregulated eIF4E-dependent translational control. Nature. Jan 17 2013;493(7432):371-7. doi:10.1038/nature11628

16. Kouloulia S, Hallin EI, Simbriger K, et al. Raptor-Mediated Proteasomal Degradation of Deamidated 4E-BP2 Regulates Postnatal Neuronal Translation and NF-kappaB Activity. Cell Rep. Dec 10 2019;29(11):3620-3635 e7. doi:10.1016/j.celrep.2019.11.023

17. Simbriger K, Amorim IS, Chalkiadaki K, et al. Monitoring translation in synaptic fractions using a ribosome profiling strategy. J Neurosci Methods. Jan 1 2020;329:108456. doi:10.1016/j.jneumeth.2019.108456

18. Ingolia NT, Lareau LF, Weissman JS. Ribosome profiling of mouse embryonic stem cells reveals the complexity and dynamics of mammalian proteomes. Cell. Nov 11 2011;147(4):789-802. doi:10.1016/j.cell.2011.10.002

19. Quackenbush J. Microarray data normalization and transformation. Nat Genet. Dec 2002;32 Suppl:496-501. doi:10.1038/ng1032

20. Xiao Z, Zou Q, Liu Y, Yang X. Genome-wide assessment of differential translations with ribosome profiling data. Nat Commun. Apr 4 2016;7:11194. doi:10.1038/ncomms11194

21. Reimand J, Arak T, Adler P, et al. g:Profiler-a web server for functional interpretation of gene lists (2016 update). Nucleic Acids Res. Jul 08 2016;44(W1):W83-9. doi:10.1093/nar/gkw199

22. Pascovici D, Handler DC, Wu JX, Haynes PA. Multiple testing corrections in quantitative proteomics: A useful but blunt tool. Proteomics. Sep 2016;16(18):2448-53. doi:10.1002/pmic.201600044

23. Frey U, Krug M, Reymann KG, Matthies H. Anisomycin, an inhibitor of protein synthesis, blocks late phases of LTP phenomena in the hippocampal CA1 region in vitro. Brain Res. Jun 14 1988;452(1-2):57-65.

24. English JD, Sweatt JD. A requirement for the mitogen-activated protein kinase cascade in hippocampal long term potentiation. J Biol Chem. Aug 01 1997;272(31):19103-6.

25. Ingolia NT, Ghaemmaghami S, Newman JR, Weissman JS. Genome-wide analysis in vivo of translation with nucleotide resolution using ribosome profiling. Science. Apr 10 2009;324(5924):218-23. doi:10.1126/science.1168978

26. Furic L, Rong L, Larsson O, et al. eIF4E phosphorylation promotes tumorigenesis and is associated with prostate cancer progression. Proc Natl Acad Sci U S A. Aug 10 2010;107(32):14134-9. doi:10.1073/pnas.1005320107

27. Chou MF, Schwartz D. Biological sequence motif discovery using motif-x. Curr Protoc Bioinformatics. Sep 2011;Chapter 13:Unit 13 15-24. doi:10.1002/0471250953.bi1315s35

28. Beurel E, Grieco SF, Jope RS. Glycogen synthase kinase-3 (GSK3): regulation, actions, and diseases. Pharmacol Ther. Apr 2015;148:114-31. doi:10.1016/j.pharmthera.2014.11.016

29. Sang Y, Li Y, Zhang Y, et al. CDK5-dependent phosphorylation and nuclear translocation of TRIM59 promotes macroH2A1 ubiquitination and tumorigenicity. Nat Commun. Sep 5 2019;10(1):4013. doi:10.1038/s41467-019-12001-2

30. Carlson SM, Chouinard CR, Labadorf A, et al. Large-scale discovery of ERK2 substrates identifies ERK-mediated transcriptional regulation by ETV3. Sci Signal. Oct 25 2011;4(196):rs11. doi:10.1126/scisignal.2002010

31. Ascano M, Jr., Mukherjee N, Bandaru P, et al. FMRP targets distinct mRNA sequence elements to regulate protein expression. Nature. Dec 20 2012;492(7429):382-6. doi:10.1038/nature11737

32. Darnell JC, Van Driesche SJ, Zhang C, et al. FMRP stalls ribosomal translocation on mRNAs linked to synaptic function and autism. Cell. Jul 22 2011;146(2):247-61. doi:10.1016/j.cell.2011.06.013

33. Thoreen CC, Chantranupong L, Keys HR, Wang T, Gray NS, Sabatini DM. A unifying model for mTORC1-mediated regulation of mRNA translation. Nature. May 2 2012;485(7396):109-13. doi:10.1038/nature11083

34. Gamache TR, Araki Y, Huganir RL. Twenty Years of SynGAP Research: From Synapses to Cognition. J Neurosci. Feb 19 2020;40(8):1596-1605. doi:10.1523/JNEUROSCI.0420-19.2020

35. Walkup WGt, Washburn L, Sweredoski MJ, et al. Phosphorylation of synaptic GTPase-activating protein (synGAP) by Ca2+/calmodulin-dependent protein kinase II (CaMKII) and cyclin-dependent kinase 5 (CDK5) alters the ratio of its GAP activity toward Ras and Rap GTPases. J Biol Chem. Feb 20 2015;290(8):4908-27. doi:10.1074/jbc.M114.614420

36. Meili F, Wei WJ, Sin WC, et al. Multi-parametric analysis of 57 SYNGAP1 variants reveal impacts on GTPase signaling, localization, and protein stability. Am J Hum Genet. Jan 7 2021;108(1):148-162. doi:10.1016/j.ajhg.2020.11.011

37. Walkup WGt, Washburn L, Sweredoski MJ, et al. Phosphorylation of synaptic GTPase-activating protein (synGAP) by Ca2+/calmodulin-dependent protein kinase II (CaMKII) and cyclin-dependent kinase 5 (CDK5) alters the ratio of its GAP activity toward Ras and Rap GTPases. J Biol Chem. Feb 20 2015;290(8):4908-4927. doi:10.1074/jbc.M114.614420

38. Xie J, Merrett JE, Jensen KB, Proud CG. The MAP kinase-interacting kinases (MNKs) as targets in oncology. Expert Opin Ther Targets. Mar 2019;23(3):187-199. doi:10.1080/14728222.2019.1571043

39. Megat S, Ray PR, Moy JK, et al. Nociceptor Translational Profiling Reveals the Ragulator-Rag GTPase Complex as a Critical Generator of Neuropathic Pain. J Neurosci. Jan 16 2019;39(3):393-411. doi:10.1523/JNEUROSCI.2661-18.2018

40. Reich SH, Sprengeler PA, Chiang GG, et al. Structure-based Design of Pyridone-Aminal eFT508 Targeting Dysregulated Translation by Selective Mitogen-activated Protein Kinase Interacting Kinases 1 and 2 (MNK1/2) Inhibition. J Med Chem. Apr 26 2018;61(8):3516-3540. doi:10.1021/acs.jmedchem.7b01795

41. Kopanitsa MV, Gou G, Afinowi NO, Bayes A, Grant SGN, Komiyama NH. Chronic treatment with a MEK inhibitor reverses enhanced excitatory field potentials in Syngap1(+/-) mice. Pharmacol Rep. Aug 2018;70(4):777-783. doi:10.1016/j.pharep.2018.02.021

42. Gantois I, Khoutorsky A, Popic J, et al. Metformin ameliorates core deficits in a mouse model of fragile X syndrome. Nat Med. Jun 2017;23(6):674-677. doi:10.1038/nm.4335

43. Aguilar-Valles A, Haji N, De Gregorio D, et al. Translational control of depression-like behavior via phosphorylation of eukaryotic translation initiation factor 4E. Nat Commun. Jun 25 2018;9(1):2459. doi:10.1038/s41467-018-04883-5

44. Waskiewicz AJ, Flynn A, Proud CG, Cooper JA. Mitogen-activated protein kinases activate the serine/threonine kinases Mnk1 and Mnk2. EMBO J. Apr 15 1997;16(8):1909-20. doi:10.1093/emboj/16.8.1909

45. Bai X, Ma D, Liu A, et al. Rheb activates mTOR by antagonizing its endogenous inhibitor, FKBP38. Science. Nov 9 2007;318(5852):977-80. doi:10.1126/science.1147379

46. Morita M, Prudent J, Basu K, et al. mTOR Controls Mitochondrial Dynamics and Cell Survival via MTFP1. Mol Cell. Sep 21 2017;67(6):922-935 e5. doi:10.1016/j.molcel.2017.08.013

47. Brown MC, Gromeier M. MNK Controls mTORC1:Substrate Association through Regulation of TELO2 Binding with mTORC1. Cell Rep. Feb 7 2017;18(6):1444-1457. doi:10.1016/j.celrep.2017.01.023

48. Lineham E, Spencer J, Morley SJ. Dual abrogation of MNK and mTOR: a novel therapeutic approach for the treatment of aggressive cancers. Future Med Chem. Sep 2017;9(13):1539-1555. doi:10.4155/fmc-2017-0062

49. Agarwal M, Johnston MV, Stafstrom CE. SYNGAP1 mutations: Clinical, genetic, and pathophysiological features. Int J Dev Neurosci. Nov 2019;78:65-76. doi:10.1016/j.ijdevneu.2019.08.003

50. Sato A. mTOR, a Potential Target to Treat Autism Spectrum Disorder. CNS Neurol Disord Drug Targets. 2016;15(5):533-43. doi:10.2174/1871527315666160413120638

51. Rosina E, Battan B, Siracusano M, et al. Disruption of mTOR and MAPK pathways correlates with severity in idiopathic autism. Transl Psychiatry. Jan 31 2019;9(1):50. doi:10.1038/s41398-018-0335-z

Figure legends

Figure 1 Mnk1/2 depletion impairs synaptic plasticity, learning and memory. a. Morris water maze (MWM) task. Left: graphic depiction of experimental design; latency (s) to find hidden platform during experimental days. Right: Platform crossings and quadrant occupancy during probe test on day 6; Two-way ANOVA, with Tukey's post-hoc, **b.** Contextual fear conditioning. Top: Experimental outline, bottom: Percentage freezing 24 h after initial training, Student's *t*-test, **c.** Social approach and preference for social novelty (three-chamber test). Time spent sniffing the social (S1: stranger 1, S2: stranger 2) or non-social stimulus (E: Empty), Two-way ANOVA with Bonferroni's post-hoc, **d.** Self-grooming. Total time grooming and number of grooming bouts are shown, Student's *t*-test. **e.** CA1 late-LTP (L-LTP) recordings in response to theta burst stimulation (TBS) in Mnk DKO mice. Normalized fEPSP slope over 240 min. **f.** Quantification of percentage potentiation during the last 10 min, Student's *t*-test. For a-d, all data are shown as mean ± S.E.M.; *$p < 0.05$, **$p < 0.01$, ***$p < 0.001$. Mnk DKO: $Mnk1^{-/-}Mnk2^{-/-}$, WT: $Mnk1^{+/+}Mnk2^{+/+}$. See also Supplementary Table 9 for Statistical analysis details.

Figure 2 Altered translational landscape in Mnk DKO whole brain. a. Experimental design for genome-wide profiling of mRNA translation with RNA sequencing in WT and Mnk DKO mouse whole brain. **b.** Scatter plot showing $\log_2$RPKM of translationally (DTG; FDR < 0.15) or transcriptionally (DEG; FDR < 0.1) upregulated (red) and downregulated (blue) mRNAs in WT versus Mnk DKO libraries; black dots depict unchanged mRNAs; n = 2 for footprints and mRNA). **c.** Comparison of translational profiling in Mnk DKO (in **b**.) with $Eif4e^{Ser209Ala}$ribosome profiling data from Amorim *et al.*[9]. Left: Scatter plot comparing $\log_2$RPKM; blue: Mnk DKO, Orange: $Eif4e^{Ser209Ala}$ datasets and DTGs; R^2: Pearson correlation between depicted datasets. Right: Gene Ontology Analysis using DAVID for 20 common DTG between the depicted RPF datasets. Mnk DKO: $Mnk1^{-/-}Mnk2^{-/-}$, $eIF4E^{Ser209Ala}$: $Eif4e^{Ala209/Ala209}$ WT: $Mnk1^{+/+}Mnk2^{+/+}$ or $Eif4e^{Ser209/Ser209}$. Also see Supplementary Figs 1, 2 and Supplementary Tables 1, 2.

Figure 3 Mnk1/2 deletion remodels whole brain and synaptic phosphoproteome. a. Experimental design for phosphoproteome analysis of whole brain samples in WT and Mnk

DKO mouse. Volcano plot showing in red significantly altered phosphopeptides identified in Mnk DKO mouse compared with WT. X-axis demonstrates the log-transformed fold change in abundance (WT/DKO) and the Y-axis indicates the log-transformed *p* values (*t*-test) associated with individual phosphopeptides. A cut-off of log2 fold-change (dashed vertical lines) and *p* value 0.05 (dashed horizontal line) was applied. **b.** Top ranked identified consensus motif using the Motif-x package on phosphosites significantly downregulated in the Mnk DKO whole brain. **c.** Functional annotation of proteins with reduced phosphorylation (*p* value < 0.05) in Mnk DKO whole brain by DAVID. GO terms for Molecular Functions (MF), Biological Processes (BP), and Cellular Component (CC) are shown. **d.** Upstream kinase prediction analysis using the Ingenuity Pathway Analysis (IPA) package for unannotated phosphosites with 2-fold change in DKO whole brain compared with WT. **e.** Experimental design for phosphoproteome analysis of synaptosome samples in WT and Mnk DKO mouse. Volcano plot showing significantly altered phosphoproteins identified in Mnk DKO mouse compared with WT. X-axis demonstrates the log-transformed fold change in abundance (WT/DKO) and the Y-axis indicates the log-transformed *p* values (*t*-test) associated with individual phosphopeptides. A cut-off of ±2 fold-change (dashed vertical lines) and *p* value 0.05 (dashed horizontal line) was applied. **f.** The top ranked identified consensus motif using the Motif-x package on phosphosites significantly downregulated in the Mnk DKO synaptosomes. **g.** Functional annotation of proteins with reduced phosphorylation (*p* value < 0.05) in Mnk DKO synaptosomes by DAVID. Overrepresented GO terms for Molecular Functions (MF), Biological Processes (BP), and Cellular Component (CC) are shown. **h.** Upstream kinase prediction analysis using the IPA package for unannotated phosphosites with 2-fold change in DKO synaptosome compared with WT. **i.** Annotation of top Diseases and Functions enriched among the proteins with reduced phosphorylation (*p* value < 0.05) in Mnk DKO synaptosomes using the IPA package. Mnk DKO: *Mnk1*$^{-/-}$*Mnk2*$^{-/-}$ WT: *Mnk1*$^{+/+}$*Mnk2*$^{+/+}$. Also see Supplementary Figs 2,3,4,5 and Supplementary Table 3,4,5,6.

Figure 4 Mnk1/2 deletion alters synaptic translation. a. Experimental design for genome-wide profiling of mRNA translation with RNA sequencing in WT and Mnk DKO mouse synaptosomes. Scatter plot showing $\log_2$RPKM of translationally (DTG) upregulated (red) and downregulated (blue) mRNAs in WT versus Mnk DKO synaptosome libraries (FDR<0.15; n = 3

for footprints and mRNA). Mnk DKO: *Mnk1*$^{-/-}$*Mnk2*$^{-/-}$, WT: *Mnk1*$^{+/+}$*Mnk2*$^{+/+}$. **b.** Comparison of translational profiling between whole brain and synaptosomes (WT-Mnk DKO). Scatter plot showing $\log_2$ RPKM Mnk DKO/WT for translational efficiency. R^2: Pearson correlation between depicted datasets. Mnk DKO: *Mnk1*$^{-/-}$*Mnk2*$^{-/-}$, WT: *Mnk1*$^{+/+}$*Mnk2*$^{+/+}$. Also see Supplementary Fig. 2 and Supplementary Table 5.

Figure 5 Mnk1 binds to and phosphorylates Syngap1. a. Identification of Mnk1 protein interactome in whole brain by co-immunoprecipitation-mass-spectrometry (IP-MS). Volcano plot shows proteins co-enriched with Mnk1 using anti-Mnk1 antibody (over IgG). A cut-off of ± 3.5 log2 fold-change (dashed vertical lines) and *FDR<0.05* (dashed horizontal line) was applied. Ven diagram demonstrates the overlap between proteins co-enriched with Mnk1 and the proteins with reduced phosphosites in Mnk DKO synaptosomes. **b.** Analysis of Syngap1 phosphorylation in WT (wild type) and Mnk DKO whole brains. Proteins with phospho-Ser residues were immunoprecipitated by specific anti-phospho-Serine antibody and the presence of Syngap1 was measured by western blot. The bar graph represents the relative enrichment of Syngap1 protein in each genotype in the input and phospho-Ser-enriched fractions. n = 4 for each genotype; Students *t*-test, **p* < 0.05 **c.** (Top) Conservation of the two observed Mnk-sensitive phosphosites and the presence of the predicted enriched motif (Fig. 3**b** and **f**) on Syngap1 in the indicated species. (Bottom) Schematic of known domains of rat Syngap1 protein, positions of the validated and predicted phosphosites, and validated phosphorylation sites mediated by CDK5 and CamKIIα. **d.** Puromycin incorporation assay in HEK-293H cells transfected with wild-type or phospho-mutant (S788A) or phospho-mimetic (S788D) Syngap1. Representative immunoblot analysis of lysates probed with antisera against the indicated proteins; HSC70 is the loading control (n = 3 for each group). One-way ANOVA with Tukey's post-hoc, **p* < 0.05. **e.** Luminescence-based Syngap1 GAP activity assay for recombinant Rheb using Syngap1 mutants; One-way ANOVA with Bonferroni's post-hoc, ****p* < 0.001. **f.** Active Rheb (Rheb-GTP) immunoprecipitation-based assay. Syngap1 wild-type, mutants or empty vector groups were probed with antisera against the indicated proteins using IP and total lysates; HSC70: loading control. **g.** mTORC1 activity in synaptosomes from Mnk DKO mouse brain. (Left) Representative images from immunoblotting of synaptosome lysates probed with antisera against the indicated proteins; β-actin is the loading control. (Right) Quantification of relative protein

expression in immunoblotting experiment. Normalised expression of two phosphosites on rpS6 (240/244, 235/236) is depicted; n = 3 for each genotype. **h.** Luminescence-based Syngap1 GAP activity assay (from IP Syngap1) in brain synaptosomes. Residual GTP (indicative of GTP hydrolysis) for wild type and Mnk DKO synaptosomes. for g, h Students *t*-test, *$p < 0.05$, **$p < 0.01$. Mnk DKO: *Mnk1*$^{-/-}$*Mnk2*$^{-/-}$, WT: *Mnk1*$^{+/+}$*Mnk2*$^{+/+}$. Also see Supplementary Figures 6, 7 and Supplementary Table 7. See also Supplementary Table 9 for Statistical analysis details.

Figure 6 AAV9-mediated Syngap1 knockdown reverses memory deficits in Mnk DKO mice and pharmacological inhibition of Mnk corrects behavioural deficits in *Syngap1*$^{+/-}$ mice. a. Left: Experimental design for AAV9-mediated knock-down of *Syngap1* mRNA in mouse brain via intra-hippocampal stereotactic injection. Short-hairpin RNA (shRNA) constructs driven by the U6 promoter were expressed for 4 weeks prior to behavioural testing. Representative images from immunoblotting of hippocampus lysates from WT mice injected with scrambled or *Syngap1* shRNA expressing AAV9 for 2 or 4 weeks, probed with antisera against the indicated proteins; Hsc70 is the loading control Middle: Behavioural analysis for the indicated groups in Morris water maze (MWM). Latency to find the hidden platform (s) is shown for different days and treatments Two-way ANOVA, with Tukey's post-hoc. Right: Behavioural analysis for the indicated groups in contextual fear conditioning (CFC): Percentage freezing 24 h after initial training is shown **b.** (Left) Experimental design for eFT508 pharmacological inhibition of Mnk kinase activity in mouse brain. eFT508 (1 mg/kg, daily for 5 days) was administered via intraperitoneal injection in mice prior to behavioural testing. Behavioural analysis for the indicated groups; self-grooming: total time spent grooming, open field test: Time spent in the centre of the open field and three-chamber social interaction and preference for social novelty tests: Sociability and social novelty indices are shown. Two-way ANOVA with Bonferroni's post-hoc. **c.** Immunoblot analysis and quantification of hippocampal tissue isolated from animals analysed in a. **d.** Proposed mechanism for behavioural rescue in Mnk DKO mice by Syngap1 shRNA **e.** Immunoblot analysis and quantification from hippocampal tissue isolated from animals analysed in b. **f.** Proposed mechanism for behavioural rescue in *Syngap1*$^{+/-}$ mice by eFT508 treatment. For c, e: Representative immunoblots probed with antisera against the indicated proteins are shown; Hsc70 is the loading control. One-way ANOVA with Bonferroni's post-hoc. For a-e: All data are shown as mean ± S.E.M. *$p < 0.05$, **$p < 0.01$, ***$p < 0.001$.

Mnk DKO: *Mnk1*$^{-/-}$*Mnk2*$^{-/-}$, Syngap1+/-: *Syngap1*$^{+/-}$, WT: *Mnk1*$^{+/+}$*Mnk2*$^{+/+}$ or *Syngap1*$^{+/+}$. See also Supplementary Figure 8 and Supplementary Table 9 for Statistical analysis details.

Figure 7 Proposed mechanisms for the Mnk-Syngap1 interplay. Syngap1 phosphorylation by Mnk is a new translational control pathway downstream of MAPK, regulating memory and autism-related behaviours, while eIF4E phosphorylation is important for translation of mRNAs coding for extracellular matrix (ECM) proteins. **Left,** Syngap1 is an inhibitor of mTORC1, controlling Protein Synthesis and Memory and Autism-related behaviours. Mnks phosphorylate Syngap1 on S788 to reduce its GAP activity for Rheb and thus promote mTORC1 activity and protein synthesis, which are required for memory and autism-related behaviours. **Right,** Depletion of Mnks reduces Syngap1 S788 phosphorylation, increasing Syngap1 inhibitory GAP activity, reducing active Rheb and thus decreasing mTORC1 activity and protein synthesis, leading to memory impairment and autism-related behaviours.

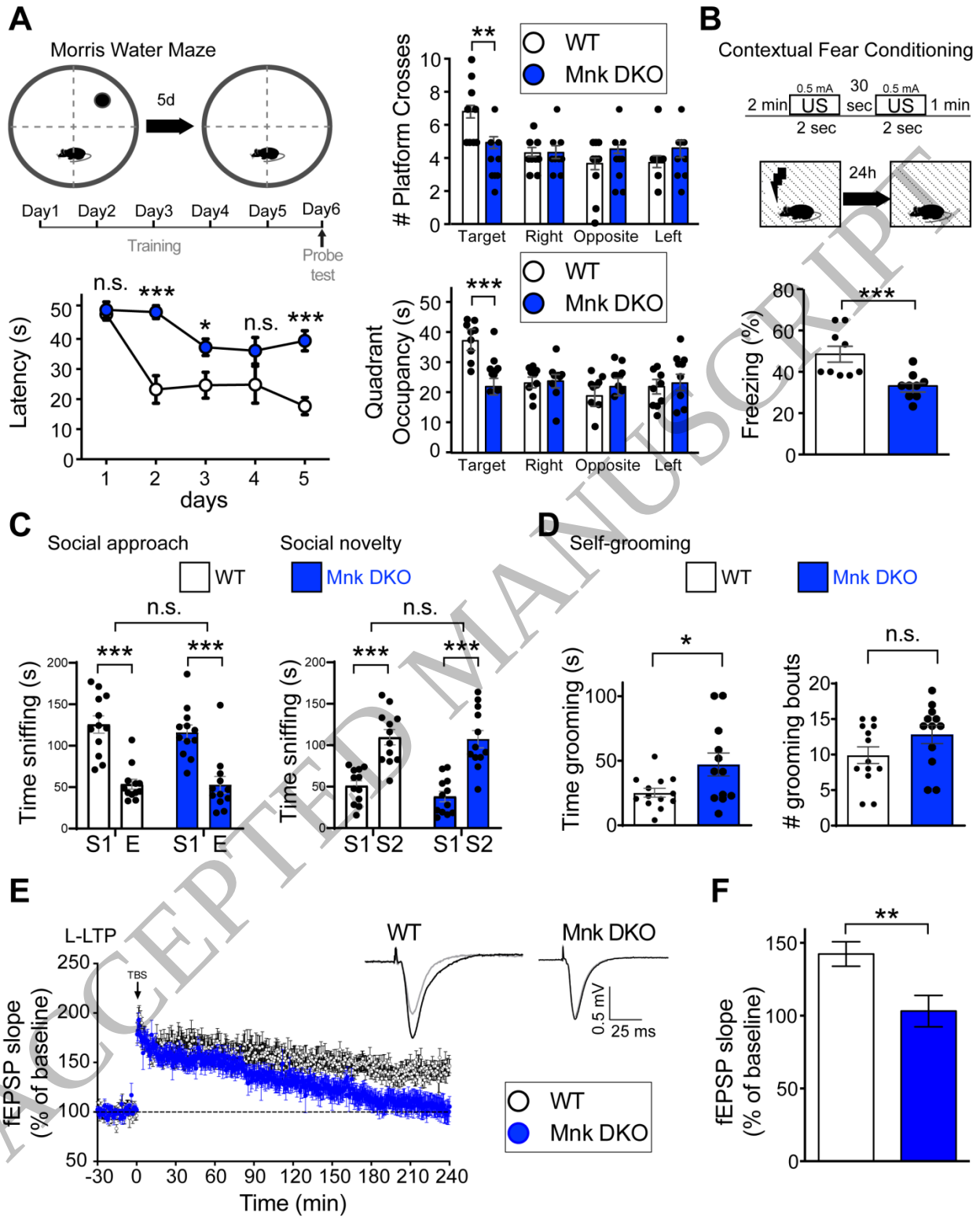

Figure 1
210x263 mm (.59 x DPI)

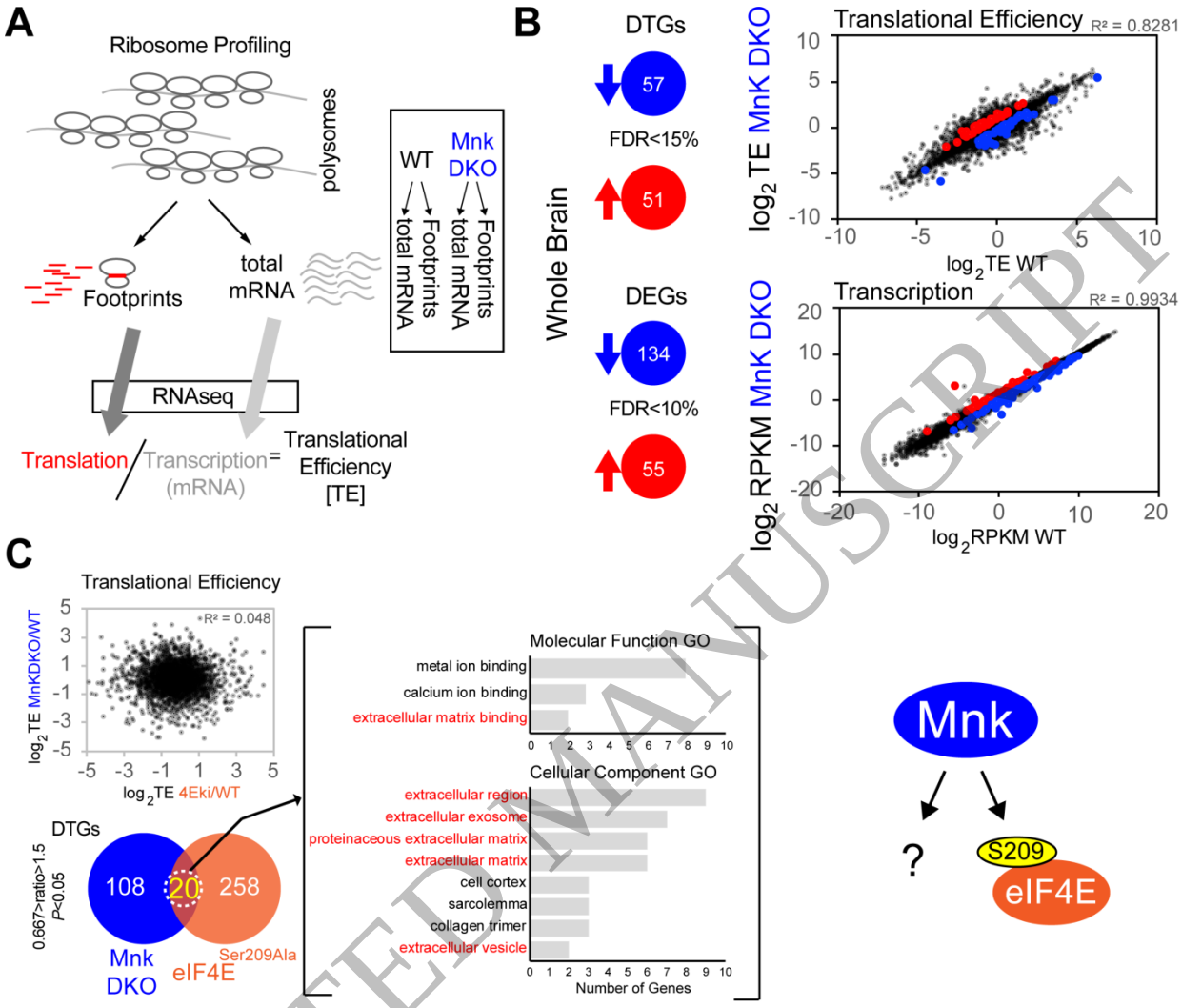

Figure 2
206x178 mm (.59 x DPI)

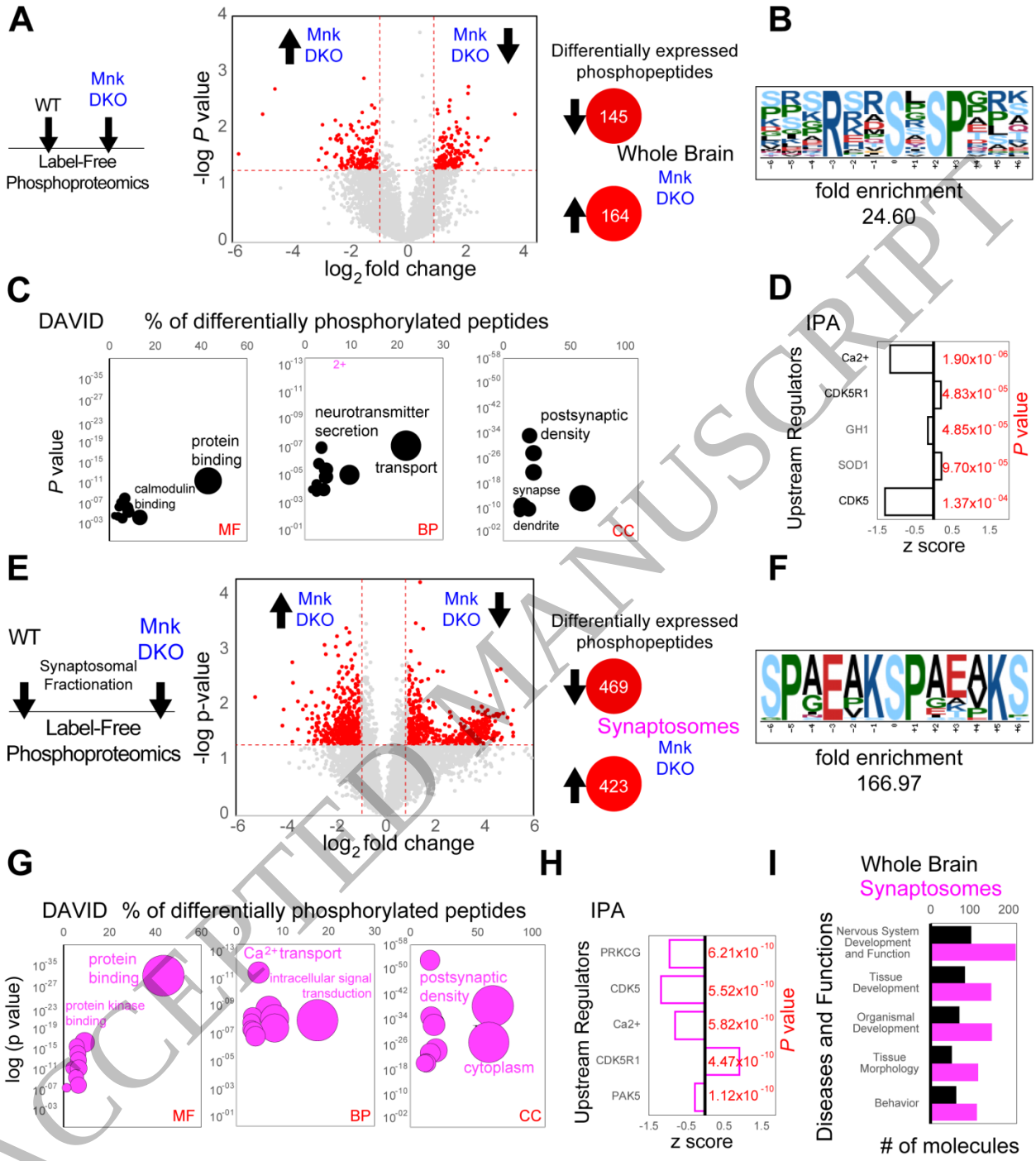

Figure 3
208x235 mm (.59 x DPI)

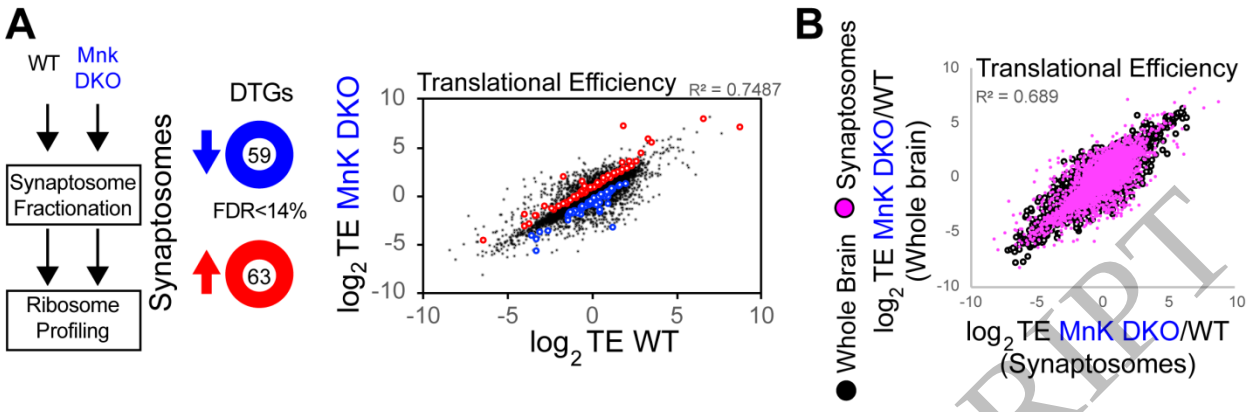

Figure 4
206x68 mm (.59 x DPI)

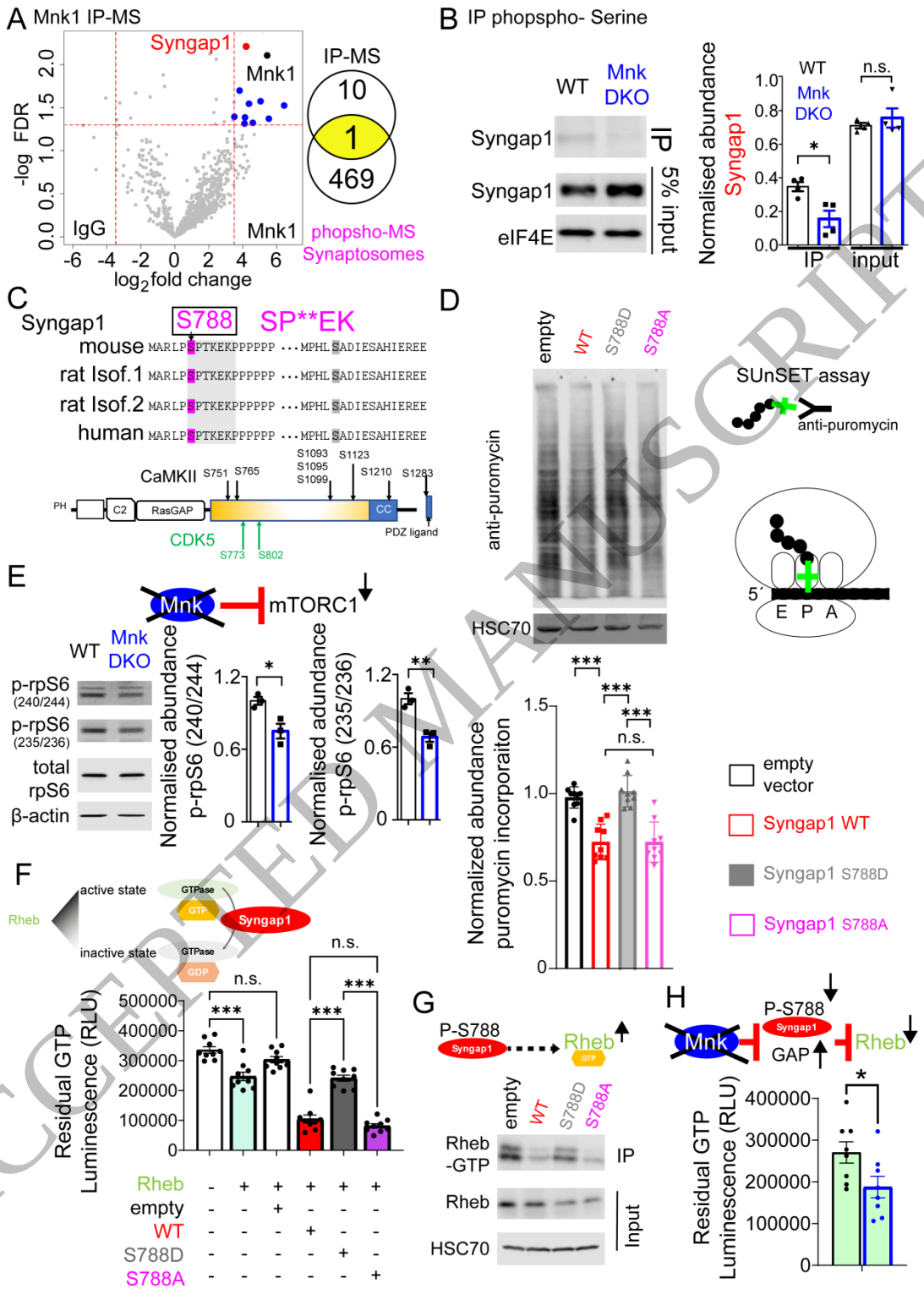

Figure 5
209x298 mm (.59 x DPI)

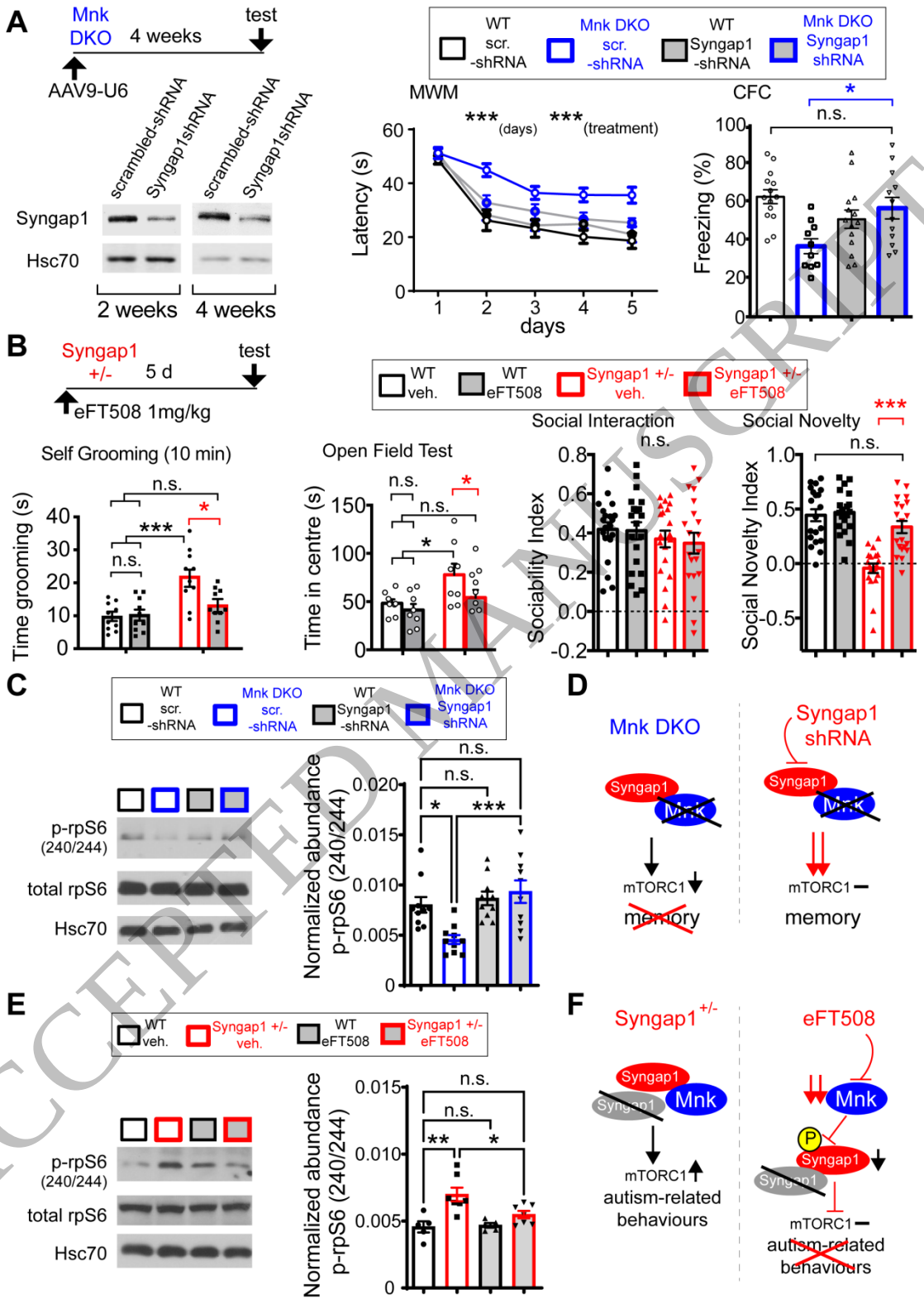

Figure 6
207x295 mm (.59 x DPI)

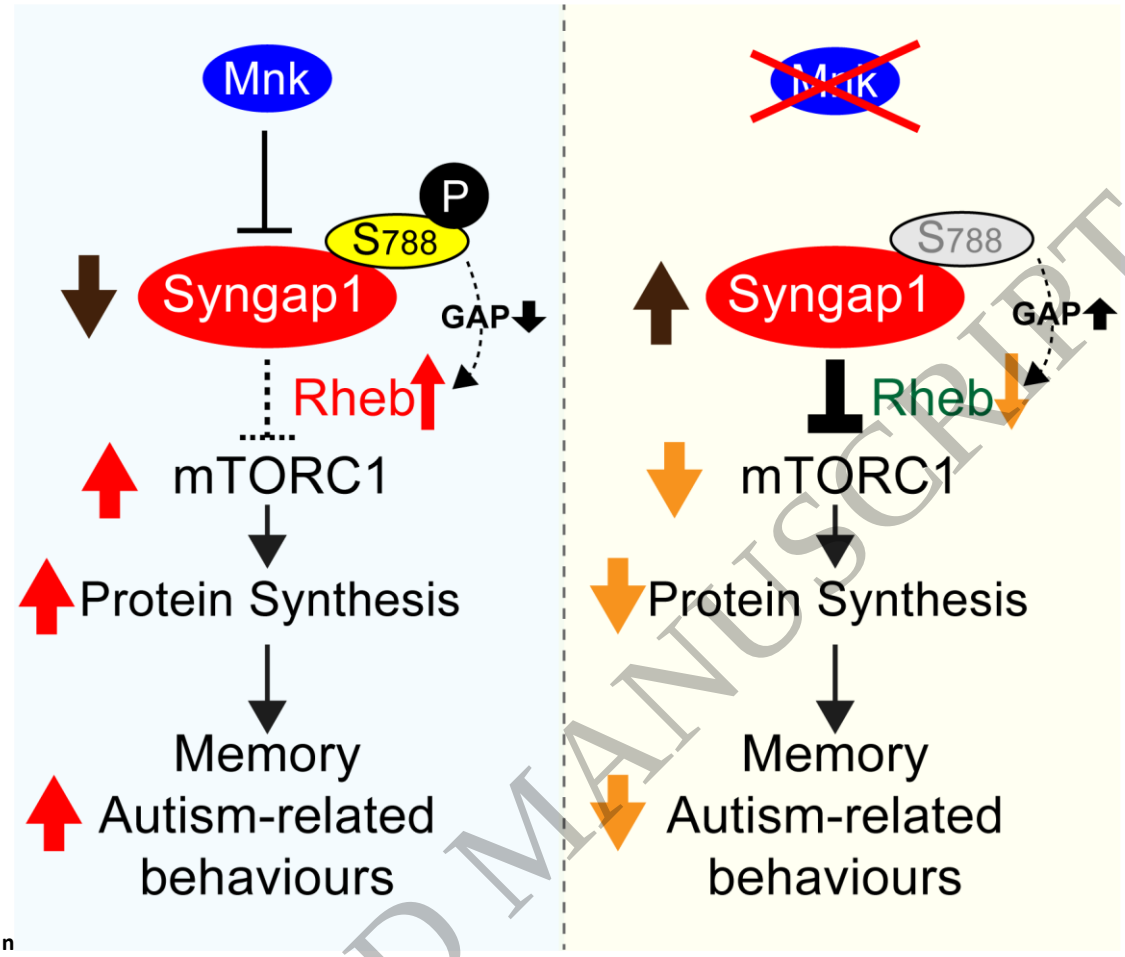

n

Figure 7
146x125 mm (.59 x DPI)